Glial ferritin maintains neural stem cells via transporting iron required for self-renewal in *Drosophila*

Zhixin Ma,[1] Wenshu Wang,[1] Xiaojing Yang,[1] Menglong Rui,[1] Su Wang [1,2,3,*]

[1]School of Life Science and Technology, The Key Laboratory of Developmental Genes and Human Disease, Ministry of Education, Southeast University, 2 Sipailou Road, Nanjing 210096, China

[2]Co-innovation Center of Neuroregeneration, Nantong University, Nantong, China

[3]Lead Contact

[*]Correspondence: wangsu@seu.edu.cn

Abstract

Stem cell niche is critical for regulating the behavior of stem cells. Drosophila neural stem cells (Neuroblasts, NBs) are encased by glial niche cells closely, but it still remains unclear whether glial niche cells can regulate the self-renewal and differentiation of NBs. Here we show that ferritin produced by glia, cooperates with Zip13 to transport iron into NBs for the energy production, which is essential to the self-renewal and proliferation of NBs. The knockdown of glial ferritin encoding genes causes energy shortage in NBs via downregulating aconitase activity and NAD^+ level, which leads to the low proliferation and premature differentiation of NBs mediated by Prospero entering nuclei. More importantly, ferritin is a potential target for tumor suppression. In addition, the level of glial ferritin production is affected by the status of NBs, establishing a bicellular iron homeostasis. In this study, we demonstrate that glial cells are indispensable to maintain the self-renewal of NBs, unveiling a novel role of the NB glial niche during brain development.

Keywords: glia, ferritin, neural stem cells, iron homeostasis, self-renewal

Introduction

Neural stem cells (NSCs) possess the remarkable ability to self-renew for maintaining their identity and differentiate into diverse neural cell types required for neurogenesis during brain development. The self-renewal, differentiation, and proliferation of NSCs are regulated by both intrinsic programs inside stem cells and extrinsic cues from the surrounding niches. The mammalian NSC niche found in the neurogenic regions is composed of diverse cell types including choroid plexus, vascular endothelia cells, pericytes, microglia, and meninges, which regulate NSC behaviors such as proliferation, self-renewal, and differentiation (Bjornsson, Apostolopoulou, Tian, & Temple, 2015). The diversity and complexity of these cell populations confer niche the ability of integrating local and systemic signals, but make it complicated to study the interaction between niches and NSCs in mammals, which is a critical issue to understand neurogenesis and improve clinical applications of NSCs.

Drosophila larval central nervous system (CNS), composed of central brain (CB), optic lobe (OL) and ventral nerve cord (VNC), is a simple but sophisticated model to decipher the regulatory mechanisms underlying NSC behaviors mediated by niche signals. In this system, *Drosophila* NSCs, called neuroblasts (NBs), and their progenies are encased by a variety of glial cells including perineurial glia, subperineurial glia, cortex glia, astrocyte-like glia and ensheathing glia

(Hartenstein, 2011; Ito, Urban, & Technau, 1995; Pereanu, Shy, & Hartenstein, 2005). These glial cells not only form the physical support structure for NBs, but also provide extrinsic cues that regulate NB reactivation, survival, and proliferation (Read, 2018; Speder & Brand, 2014). However, it remains elusive whether the glial-cell-forming niche is involved in the regulation of the prominent characteristics of NBs, self-renewal and differentiation.

Iron is a vital micronutrient for almost all living organisms since it participates in many crucial biological processes, including mitochondrial electron transport and cellular respiration that both support ATP production used for most cellular activities. High levels of iron are found in many organs including the brain, where iron is required for myelination and formation of neuronal dendritic trees (Lozoff et al., 2006; Moller et al., 2019; Rice & Barone, 2000). Iron deficiency in infants and early childhood has been well documented to be associated with long-term cognitive, social, and emotional problems (Fretham, Carlson, & Georgieff, 2011). Thus, it is intriguing to investigate whether iron is also required in NSCs during neurogenesis.

Ferritin, a ubiquitous protein present in most organisms, is composed of 24 subunits that assemble into a hollow-sphere complex capable of storing up to 4,500 iron atoms in a bioavailable form (Andrews, 2005; Knovich, Storey, Coffman, Torti, & Torti, 2009). Ferritin in both mammal and insect is a heteropolymer, consisting of heavy and light chain homologue subunits. In *Drosophila*, these subunits are encoded by *ferritin 1 heavy chain homologue* (*Fer1HCH*) and *ferritin 2 light chain homologue* (*Fer2LCH*) respectively (Arosio, Ingrassia, & Cavadini, 2009; Pham & Winzerling, 2010), which both contain secretion signal peptides that direct them to the ER during translation (Lind, Ekengren, Melefors, & Soderhall, 1998). Consequently, *Drosophila* ferritin is confined to the secretory pathway and abundant in the hemolymph (Nichol, Law, & Winzerling, 2002). Ferritin or iron manipulation in *Drosophila* glia regulate the adult behavior, such as locomotion (Kosmidis et al., 2011; Navarro, Botella, Metzendorf, Lind, & Schneuwly, 2015). Previous researches have shown that *Drosophila* ferritin not only directly participates in dietary iron absorption by removing iron from enterocytes across the basolateral membrane, but competes with transferrin to deliver iron between the gut and the fat body (Tang & Zhou, 2013; Xiao, Liu, Zhao, Wang, & Zhou, 2019). These findings underscore the pivotal role of ferritin in iron transport. Interestingly, iron-loaded ferritin, serving as an essential mitogen, promotes proliferation of cultured *Drosophila* cells (Li, 2010). Therefore, it is tempting to investigate whether ferritin is required for self-renewal and proliferation of NSCs during brain development.

Here we show that glial ferritin supplies iron into NBs to form iron-sulfur (Fe-S) clusters, which is necessary for the production of ATP, providing the energy required for self-renewal and proliferation of NBs, highlighting ferritin as a potential target for suppressing tumor.

Results

Glial ferritin is required for NB maintenance and proliferation

To identify new niche factors involved in the balance between NB self-renewal and differentiation, we used *repo-GAL4* to perform an RNAi mediated screen in glial cells. *Fer1HCH* and *Fer2LCH*, two ferritin subunit encoding genes, were identified to be essential for NB maintenance and brain development. Specifically, knocking down *Fer1HCH* or *Fer2LCH* in glial cells significantly reduced the number of NBs in the CB and VNC at the third-instar larval stage, which resulted in decreased size of the CNS (**Figure 1A and B and Figure 1-figure supplement 1A**). To further assess the impact on NB proliferation, we employed the mitotic marker phosphohistone H3 (PH3)

and the thymidine analogue 5-ethynyl-2'-deoxyuridine (EdU), revealing a substantial decrease in the proliferation rate of NBs upon glial ferritin knockdown (**Figure 1A and C and Figure 1-figure supplement 1B and C**). These results indicated that glial ferritin is required for maintaining NBs and their proliferation.

To identify the glial subpopulation in which ferritin functions, we employed subtype-restricted GAL4 to perform ferritin knockdowns (**Table 1**). We observed that knocking down ferritin genes in cortex glia led to a similar yet milder phenotype compared to that observed in the pan-glia knockdown (**Figure 1-figure supplement 1D**). This milder effect may be attributed to potential compensatory mechanisms from other glial subpopulations. Interestingly, knocking down ferritin in other glial subtypes did not yield any discernible phenotype (**Figure 1—figure supplement 2**). These findings suggest that ferritin functions collectively across all glial populations to regulate the activity of NBs.

We confirmed the phenotype with multiple independent RNAi lines for *Fer1HCH* or *Fer2LCH*, and observed similar abnormalities of larval NBs and brain development (**Figure 1-figure supplement 3A**). Hereafter, *UAS-Fer1HCH-RNAi* (THU5585) and *UAS-Fer2LCH-RNAi* (TH01861.N) were used for most studies, and we only quantified NB number and proliferation rate in the CB for convenience in this research.

To evaluate the efficiency of RNAi for *Fer1HCH* or *Fer2LCH*, RT-PCR was performed with total RNA isolated from whole brain dissected from third-instar larvae. The abundance of *Fer1HCH* or *Fer2LCH* mRNA was significantly reduced in glial *Fer1HCH* or *Fer2LCH* knockdown respectively (**Figure 1D and E**). Western blot analysis of larval brain protein extract using polyclonal antibodies against Fer1HCH or Fer2LCH further confirmed that both subunits were down-regulated in glial knockdown of either subunit (**Figure 1F-I**), consistent with previous research in *Drosophila* (Missirlis et al., 2007). To exclude the possibility of RNAi off-target effects, we used *repo-GAL4* to overexpress RNAi-resistant *Fer1HCH* (or *Fer2LCH*) containing silent mutations in the region targeted by shRNA, which resulted in a significant increase in the number and proliferation rate of NBs compared to glial ferritin knockdown alone (**Figure 1J-L and Figure 1-figure supplement 3B and C**). Additionally, similar but weaker phenotypes were observed when $Fer1HCH^{DN}$, a ferroxidase-inactive form of Fer1HCH (Missirlis et al., 2007), was overexpressed in glial cells (**Figure 1-figure supplement 3D**). These results support the conclusion that ferritin in glial cells is essential for the maintenance and proliferation of NBs, suggesting that iron homeostasis is involved in this process.

Ferritin is produced mainly in glial cells and secreted into NBs through a vesicle-dependent pathway

To investigate the role of iron homeostasis in *Drosophila* CNS, we tried to knock down genes involved in iron transport, storage, and regulation in NBs, neurons, and glial cells, respectively. Interestingly, only glial knockdown of ferritin-related genes led to NB loss and defective brain development. It appears that ferritin generated in glial cells is the only crucial protein for regulating the behavior of NBs and, ultimately, the larval brain development. To recapitulate the endogenous ferritin expression pattern, we took advantage of a Fer1HCH/Fer2LCH enhancer trapped GAL4 line to drive a variant of DsRed protein with a nuclear localization signal (DsRed Stinger). Surprisingly, our immunostaining experiments revealed that most, if not all, DsRed was co-localized with the glia nuclear protein Repo, instead of the NB nuclear protein Dpn (**Figure 2A**

and A'). We also used another Fer2LCH enhancer trapped GAL4 line to verify this result, which was consistent with above result (**Figure 2—figure supplement 1**). These results further confirm that glial cells are the main producers of ferritin in the larval brain.

Fer1HCH^{G188} encodes a GFP-tagged Fer1HCH subunit (Missirlis et al., 2007), which labels the distribution of Fer1HCH, representing the pattern of ferritin. As shown in the **Figure 2B and B'**, ferritin was detected in NBs besides glial cells, despite that ferritin is specifically produced in glial cells. To explore the possibility of ferritin transfer from glial cells to NBs, we observed the GFP signal of *Fer1HCH*^{G188} with glial ferritin knockdown, and found that GFP in the brain was almost completely depleted (**Figure 2B**). Furthermore, we used *repo-GAL4* to drive the expression of GFP-tagged Fer1HCH and mCherry-tagged Fer2LCH in glial cells. We observed that both Fer1HCH::GFP and Fer2LCH::mCherry were present in NBs, while the control GFP and mCherry were restricted to glial cells (**Figure 2C**). Altogether, we conclude that ferritin is generated in glial cells and then transferred to NBs in the larval brain.

In *Drosophila*, both ferritin subunits contain secretion signal peptides that direct protein to the endoplasmic reticulum during translation, which allows the ferritin to be transported out of the cell. To investigate whether the ferritin was transported from glia to NBs via the vesicular transport, we expressed a temperature-sensitive dominant-negative Shibire dynamin protein (shi^{ts}) to block vesicle trafficking from glial cells, and found that Fer1HCH::GFP accumulated in glia, accompanying with significantly diminished Fer1HCH signal in NBs (**Figure 2D, D' and E**), suggesting glial ferritin secretes into NBs through vesicle system.

Glial ferritin defects lead to iron deficiency in NBs

Given that ferritin is required for iron storage as well as delivery, glial ferritin knockdown might increase free iron level, leading to glial iron overload. Alternatively, it will block the iron transport from glia to NBs, resulting in NB iron deficiency. To determine the underlying cause of the brain development defects observed upon glial ferritin knockdown, we used iron chelator or iron salt ferric ammonium citrate (FAC) to manipulate iron intake and detect how it will influence NBs. We observed that depriving iron intake by adding iron chelator bathophenanthrolinedisulfonic acid disodium (BPS) to the food led to a dramatic decrease in the number and proliferation rate of NBs, compared to control larvae on normal food (**Figure 3A**). To investigate the effect of feeding behavior in different food, we tested the feeding behavior of fly by incorporating 1% Brilliant Blue (sigma, 861146) into different food (Tanimura, Isono, Takamura, & Shimada, 1982) and found the amount of dye in the fly body was similar between normal group and BPS group (**Figure 3—figure supplement 1A**), which suggested that BPS almost did not affect the feeding behavior. In line with this result, blocking iron absorption by knocking down intestinal ferritin (Tang & Zhou, 2013) resulted in the similar defects of brain (**Figure 3-figure supplement 1B-D**). However, supplementing the diet with FAC did not induce any observable defects (**Figure 3A**). We also tested another iron chelator deferiprone (DFP) (Soriano et al., 2013), and found that DFP alone did not cause any brain defects in wild-type (WT) larvae, but it significantly exacerbated the effect of glial ferritin knockdown on defective NB maintenance (**Figure 3B and C**). Furthermore, we attempted to rescue the brain defects observed in glial ferritin knockdown by providing dietary FAC, but the effect was negligible (**Figure 3-figure supplement 1E and F**). This may be due to the possibility that the knockdown of glial ferritin largely, if not completely, prevented the transport of iron from glia to NBs, which hindered the additional iron from entering NBs. These

results indicate that the NB loss phenotype induced by glial ferritin knockdown is primarily due to iron deficiency in NBs.

Zip13, generally known as a zinc transporter, functions as an iron transporter, cooperating with ferritin on iron transport in *Drosophila* intestine (Xiao, Wan, Fan, Tang, & Zhou, 2014). Specifically, knockdown of *Zip13* leads to failure of iron loading in secretory vesicles and consequently defective iron efflux (Xiao et al., 2014). To investigate whether the NB loss phenotype of glial ferritin knockdown is caused by defective iron transport, we next sought to identify the role of Zip13 in the larval brain. Firstly, we examined the expression pattern of Zip13 and found that, similar to ferritin, the DsRed stinger driven by *Zip13-GAL4* was co-localized with Repo in glial cells rather than Dpn in NBs (**Figure 3D and D'**). Subsequently, we knocked down *Zip13* in glial cells and observed a similar but weaker phenotype with the slightly reduced NB number and proliferation rate (**Figure 3E-G**). Consistently, the defective brain development was confirmed in *Zip13* mutant (**Figure 3-figure supplement 1G-I**). Moreover, the effect of double knockdown of both *Zip13* and *Fer2LCH* was much more severe than that of either single knockdown, with a significant reduction in NB number and proliferation rate (**Figure 3E-G**). Furthermore, we found that the reduced proliferation rate caused by *Zip13* knockdown could be partially rescued by iron supplementation in the food (**Figure 3H and I**). Overall, these results suggest that glial ferritin collaborates with Zip13 to deliver iron from glia to NBs.

Since previous studies have demonstrated the essential role of glial cells in NB survival and proliferation (Bailey et al., 2015; Read, 2018), it is possible that iron overload in glial cells up-regulated the level of reactive oxygen species (ROS), leading to apoptosis of glial cells, which ultimately resulted in the loss of NBs. To rule out this possibility, firstly, we examined the ROS level of glial ferritin knockdown via a transgenic reporter GstD-GFP for oxidative stress signaling (Sykiotis & Bohmann, 2008). GstD1 is a prototypical oxidative stress response gene (Sawicki, Singh, Mondal, Benes, & Zimniak, 2003). We found an obvious increase as expected (**Figure 3-figure supplement 2A and B**). However, overexpressing anti-oxidant genes in glial cells or NBs did not restore the NB number and proliferation (**Figure 3-figure supplement 2C and D**). ROS accumulation leads to lipid peroxidation, which in turn results in ferroptosis (Hirschhorn & Stockwell, 2019). Mitochondria in cells undergoing ferroptosis typically exhibit a characteristic shrinkage and damage, while the nuclei remain structurally intact (Mumbauer, Pascual, Kolotuev, & Hamaratoglu, 2019). In order to investigate whether the NB loss is due to ferroptosis, we examined the mitochondrial morphology using Transmission Electron Microscopy (TEM). However, our result showed that the mitochondrial double membrane and cristae were clearly visible whether in the control group or glial ferritin knockdown group, which suggested that ferroptosis was not the main cause of NB loss upon glial ferritin knockdown (**Figure 3-figure supplement 2E and F**). In addition, we investigated the level of 4-HNE that indicates lipid peroxidation, the other hallmark of ferroptosis. This result showed that 4-HNE level did not change significantly after ferritin knockdown (**Figure 3-figure supplement 2G and H**), suggesting that lipid peroxidation was stable, which supported the exclusion of the ferroptosis in glial ferritin knockdown. Taken with the findings from iron chelator feeding together, we conclude that NB loss resulting from glial ferritin knockdown is not a consequence of ferroptosis. Secondly, we examined the apoptosis in larval brain cells via Caspase-3 or TUNEL staining, and found the apoptotic signal remained unchanged after glial ferritin knockdown (**Figure 3-figure supplement 3A-D**). Furthermore, we overexpressed the baculovirus protein P35 to inhibit apoptosis in glial

cells, but failed to restore the lost NBs (**Figure 3-figure supplement 3E**). Given that glial morphology is important for NB lineages (Speder & Brand, 2018), we used GFP driven by *repo-GAL4* to denote glia cells and found that glial chamber was almost intact after glial ferritin knockdown (**Figure 3-figure supplement 3F**). Together, we conclude that it is iron deficiency in NBs, rather than iron overload in glial cells, that leads to NB loss induced by ferritin defects.

Glial ferritin defects result in impaired Fe-S cluster activity and ATP production

To further prove that defective iron transport leads to the iron deficiency in NBs, we examined the iron availability by measuring aconitase activity in the brain. The activity of aconitase is sensitive to the level of Fe-S synthesis, so it can serve as an indicator for the availability of iron in the cell (Haile et al., 1992; Tong & Rouault, 2006). Aconitase activity is determined in a coupled enzyme reaction in which citrate is converted to isocitrate by aconitase (Aconitase Activity Assay Kit, sigma, MAK051). As shown in the **Figure 4A**, aconitase activity of ferritin knockdown diminished significantly, indicating that the availability of iron in the brain was reduced. This result also implies Fe-S clusters in NBs are probably deficient when knocking down ferritin in glia. Fe-S clusters are essential to activate the aconitase that converts citrate into isocitrate in the tricarboxylic acid cycle（TCA cycle) in mitochondria, and are one type of critical electron carrier for electron transport chain (ETC), especially for the Complex I, II and III function. Considering that TCA cycle and ETC are critical biological processes for ATP production, we proposed that knockdown of glial ferritin might lead to ATP deficiency due to the block of TCA cycle and ETC, which resulted in the failure of maintaining NBs and their proliferation. To verify this hypothesis, we first assessed the function of Fe-S clusters in NBs by knocking down mitochondrial Fe-S protein Nfs1 and the components of the cytosolic iron-sulfur protein assembly (CIA) complex. After knocking down *Nfs1* and the CIA component *CG17683*, *galla2*, and *ciao1* in NBs respectively, the proliferation level of NBs decreased significantly and brain size became smaller (**Figure 4B and C**), which phenocopied the knockdown of *Fer1HCH* or *Fer2LCH* in glia. This result implies that Fe-S clusters are indispensable for NBs to maintain their proliferation.

To identify the biological processes related to Fe-S clusters in NB lineages, we performed transcriptome analysis of sorted NB lineages from glial ferritin knockdown as well as the control groups. We used NB driver *Insc-GAL4* to express *UAS-DsRed*, labeling NB lineages, and then sorted these cells via fluorescence-activated cell sorting (FACS) (**Figure 4D**) (Harzer, Berger, Conder, Schmauss, & Knoblich, 2013). We found that thousands of genes were significantly altered in the *Fer1HCH* and *Fer2LCH* knockdown groups compared to the control group. Specifically, 880 genes were simultaneously downregulated among the significantly changed genes in both the *Fer1HCH* and *Fer2LCH* knockdown groups contrasted to the control group (**Figure 4E**). Given that iron deficiency in NBs probably leads to the defects of energy production and biosynthesis, we performed gene enrichment analysis in these genes based on Gene Ontology (GO) and Kyoto Encyclopedia of Genes and Genomes (KEGG). GO term analysis showed that mitochondrial organization, translation, transport, oxidative phosphorylation (OxPhos), and ETC were enriched in the Biological Processes (**Figure 4F**), indicating NB mitochondrial functions including OxPhos and ETC were abnormal after glial ferritin knockdown. Moreover, NADH dehydrogenase and ribosome related terms were also enriched whether in the Cellular Component or Molecular Function (**Figure 4F**), suggesting that NADH dehydrogenase and biosynthesis were defective. Further, we validated the enriched term associated with mitochondrial function by

qRT-PCR (**Figure 4-figure supplement 1A**). And the enriched KEGG pathways included OxPhos and ribosome (**Figure 4G**), aligning with the GO enrichment results and supporting the hypothesis that glial ferritin knockdown disrupted mitochondrial function including OxPhos and ETC as well as further biosynthesis.

To confirm whether the function of NADH dehydrogenase was disrupted, we used the SoNar that could bind to NAD^+ with specific conformation and excitatory wavelength to monitor the NAD^+ level (Bonnay et al., 2020; Zhao et al., 2016). SoNar was driven by the *Insc-GAL4* to indicate the NAD^+ level in NBs. Considering the possibility of protein accumulation in NBs due to the lower proliferation rate in glial ferritin knockdown group, the signal of SoNar was normalized to DsRed Stinger driven by *Insc-GAL4*. We observed significantly declined SoNar/DsRed after knocking down *Fer2LCH* (**Figure 4H and I**), suggesting the normalized level of NAD^+ in NBs was decreased, which supports the conclusion that the activity of NADH dehydrogenase was declined. To further verify the change of energy production, we utilized the ATP Determination Kit which offers a convenient bioluminescence assay for quantitative determination of ATP with recombinant firefly luciferase and its substrate D-luciferin. We found that ATP level decreased significantly after glial ferritin knockdown when compared to the control (**Figure 4J**). Therefore, we tried to supply the energy for NBs by restoring bioenergy-dependent NAD^+ metabolism. To validate this, we firstly determined the ATP production after overexpressing Ndi1 in NBs upon glial *Fer2LCH* knockdown. The data suggested that expression of Ndi1 can restore ATP production (**Figure 4-figure supplement 1B**). Furthermore, the NB number could be partially rescued by overexpressing proton-pump-independent yeast mitochondrial NADH dehydrogenase Ndi1 in NBs under the background of glial ferritin knockdown (**Figure 4K and L**) (Bonnay et al., 2020). In summary, the iron deficiency leads to NB loss due to the insufficient energy required for essential biological processes.

Glial ferritin maintains NBs via preventing premature differentiation

To investigate how glial ferritin knockdown leads to NB loss, we firstly examined whether NB origin was affected via altering the timing of ferritin knockdown. We used the temperature-sensitive GAL4 inhibitor $GAL80^{ts}$ to suppress ferritin RNAi at a permissive temperature (18°C) during embryonic stage, and then shifted to a restrictive temperature (29°C), or vice versa until we dissected them at the third-instar larval stage. Ferritin knockdown during the larval stage led to severe brain development defects (**Figure 5A and B**), while the knockdown only during the embryonic stage showed no apparent abnormality (**Figure 5-figure supplement 1A and B**). Together, these results indicate that glial ferritin is required for NB maintenance at the larval stage. Consistent with this result, we found no obvious defects of brain at the first-instar larval stage when knocking down glial ferritin (**Figure 5-figure supplement 1C and D**). Since newborn NBs are delaminated from the neuroectoderm during the embryonic stage (stage 9 to 11), and ferritin RNAi only during the embryonic stage did not show any phenotype, suggesting that NB loss after glial ferritin knockdown is not ascribed to defective NB origin.

Further, we explored the earliest stage when the phenotype (NB number and proliferation) existed after glial ferritin knockdown. The result showed that NB proliferation decreased significantly, but NB number declined slightly at the second-instar larval stage (**Figure 5—figure supplement 1E and F**), suggesting that brain defect of glial ferritin knockdown manifests at the second-instar larval stage.

As mentioned before, we did not detect any apoptotic signal in the larval brain after glial ferritin knockdown, suggesting that there is no association between apoptosis and NB loss. The double binary systems, lexA/lexAop and GAL4/UAS, were employed to further exclude the possibility of apoptosis. We overexpressed P35 in NBs by *Insc-GAL4* and knocked down ferritin by *repo-lexA*, which failed to restore the decreased number of NBs (**Figure 5-figure supplement 1G**). These results reinforce the notion that NB loss occurs independent of the apoptotic pathway.

Next, we hypothesized that the NB loss might be attributed to nuclear-Prospero (Pros)-dependent premature differentiation of NBs (Cabernard & Doe, 2009; Choksi et al., 2006). Pros in NB nuclear was hardly detected in third-instar WT larvae, but was increased significantly with glial ferritin knockdown (**Figure 5C and D**). To further verify that the NB loss caused by glial ferritin knockdown was due to nuclear-Pros-dependent premature differentiation, we used the *Insc-GAL4* to drive *UAS-pros-RNAi* in order to prevent the NB loss in glial ferritin knockdown background. We found that the NB number was substantially restored (**Figure 5E and F**). Interestingly, despite of dramatic NB number increase, the decreased proliferation rate was not rescued. We proposed that *pros* knockdown in NBs blocked premature terminal differentiation, but it could not replenish the reduced energy caused by glial ferritin knockdown. As NB self-renewal and proliferation are both energy-consuming processes, the self-renewal was rescued via inhibiting differentiation by *Insc-GAL4* driving *UAS-pros-RNAi*, but at the expense of energy consumption for proliferation, leaving the proliferation rate unchanged, or even lower. Together, we conclude that glial ferritin maintains the number of NBs by preventing the nuclear-Pros-dependent premature differentiation.

Furthermore, we also investigated whether overexpression of Ndi1 could restore Pros localization in NBs. This result showed that overexpressing Ndi1 could significantly restore Pros localization in NBs (**Figure 5-figure supplement 2**), which supported that energy shortage induced the entry of Pros into nuclei, leading to the premature differentiation of NBs.

Considering that asymmetric division defects in NBs may lead to premature differentiation, we also explored the asymmetric division by staining the classical asymmetric marker aPKC and found it displayed a crescent at the apical cortex based on the daughter cell position whether in control or glial ferritin knockdown (**Figure 5-figure supplement 3A**). This result indicated that there was no obvious asymmetric defect after glial ferritin knockdown.

Given that reduced proliferation is a distinctive characteristic of quiescent NBs, we tried to determine whether NBs were in a quiescent state after glial ferritin knockdown by examining the other two key features associated with quiescent NBs: decreased cell size and the formation of the extended cellular protrusions (Chell & Brand, 2010; Ly et al., 2019). However, we found that the NB size remained at the same level as control, and the extended cellular protrusion was not observed after glial ferritin knockdown (**Figure 2B' and Figure 5-figure supplement 3B**). Furthermore, since insulin signaling is necessary and sufficient to reactivate NBs from quiescence (Sousa-Nunes, Yee, & Gould, 2011), we tried to overexpress a constitutively active form of InR (InR^{act}) in NBs to promote reactivation at the background of glial ferritin knockdown. However, InR^{act} overexpression failed to ameliorate the NB abnormalities including the decreased proliferation (**Figure 5-figure supplement 3C and D**). In conclusion, NBs exhibited a low proliferation rate after glial ferritin knockdown, but were not in a quiescent state.

Ferritin functions as a potential target for tumor suppression

We have demonstrated that glial ferritin is essential for NB self-renewal and proliferation by providing glia-to-NB iron transport to support energy production in NBs. We next tried to determine whether manipulating this biological function could suppress tumor development. We induced tumor development by driving *UAS-brat-RNAi* or *UAS-numb-RNAi* under the control of *Insc-GAL4*, and knocked down ferritin genes under the control of *repo-lexA*. We observed that the size of tumors was strikingly decreased in the larval brains lacking glial ferritin (**Figure 6A and B and Figure 6- figure supplement 1A and B**). This result suggests that glial ferritin is required for tumor development, highlighting a potential target for tumor treatment.

To verify whether iron is involved in the tumor suppression induced by blocking glial ferritin, we tried to decrease iron level by adding the iron chelator BPS in the *Drosophila* food. Tumor formation in the brain at the third instar larval stage was induced with the same method as mentioned above. The addition of BPS into dietary food significantly reduced the tumor size (**Figure 6C and D and Figure 6-figure supplement 1C and D**), suggesting that iron is required for tumor development in *Drosophila* larval brain. Considering the conservation of iron's fundamental function as an essential nutrient for cell growth and proliferation, we thus tried to suppress brain tumor in mice via iron deficiency. Initially, we constructed orthotopic glioma model in C57BL/6J mice. One week after inoculation of glioma cells (GL261-luc), the iron chelator DFP was intraperitoneally injected every two days based on the murine weight until being dissected on day 7, 14, and 21, respectively. Histological examination with HE staining revealed that the size of glioma in mice, injected with DFP, decreased significantly on day 14 and 21 (**Figure 6-figure supplement 1E-G**). Since glioma cells GL261-luc carry the luciferase gene, we injected the substrate luciferin potassium salt into the tumor-bearing mice and detected the bioluminescence signal of mouse gliomas using IVIS Spectrum. This result showed that the bioluminescence signal of glioma in mice with the injection of 10 mg/ml DFP was significantly reduced (**Figure 6E and F**). The above results suggested that iron deficiency induced by DFP could suppress glioma in mice effectively. Furthermore, we assessed the survival time of the tumor-bearing mice with DFP or saline injection and found that 10 mg/ml DFP injection could significantly prolong the survival time of tumor-bearing mice (**Figure 6G**). Altogether, blocking iron into tumor is a potential therapy for tumor suppression.

Glial ferritin level is regulated by NBs

The aforementioned results have highlighted the significant role of glial ferritin in controlling NB number and proliferation. We next wonder whether NBs could provide feedback to regulate glial ferritin level. To answer this question, we analyzed ferritin level after altering NB proliferation. Previous studies have corroborated that NB proliferation was diminished by blocking Tor signaling pathway or enhanced by knocking down tumor suppressor genes, such as *brat* or *numb* (Bowman et al., 2008; Reichardt et al., 2018; Sousa-Nunes et al., 2011). When NBs were in low proliferative status, Fer2LCH subunits in the brain were significantly decreased, while Fer1HCH subunits declined slightly with no significance (**Figure 7A-D**). Conversely, highly proliferative NBs, able to form tumors, induced significantly increased level of the ferritin (**Figure 7A-D**). In summary, the production of ferritin in glial cells depends on the level of NB proliferation.

Discussion

Here we demonstrate that glia regulates iron metabolism in the brain to sustain NBs and their

proliferation. Glial ferritin coordinates Zip13 to provide iron for NBs. Once ferritin in glia is defective, NBs proliferate much slower and differentiate prematurely, implying that iron is a necessary metallic element for NBs. Iron participates in the synthesis of Fe-S clusters which activate aconitase required for TCA and facilitate electron-transfer processes involved in OxPhos. Since TCA and OxPhos are essential steps of ATP production, glial ferritin supplies iron into NBs to ensure energy production for maintaining NBs and their proliferation (**Figure 7E**).

NSCs and glial niche

Previous literatures have reported how glial niche regulates NB reactivation, proliferation, and survival. Blood-brain barrier (BBB) glia secretes dILP2 and dILP6 that bind on InR of NBs, which switches on Insulin signaling to reactivate NBs (Chell & Brand, 2010; Speder & Brand, 2014). In addition, Pvr (PDGFR ortholog) signaling in cortex glia sustains NB survival and proliferation in a PI3K-DE-cadherin-dependent manner (Read, 2018). However, it is unknown whether glial niche is required for maintaining the self-renewal of NBs. In this study, we demonstrate that glial niche maintains the self-renewal and proliferation of NBs through supplying the necessary microelement iron into NBs for enough energy production, which implies that mammalian glia likewise provides critical microelement for maintaining NSC function. Oligodendrocytes have been reported to secret ferritin to protect neuron (Mukherjee et al., 2020), however, it remains unknown whether the ferritin secretion is employed by oligodendrocytes to regulate NSCs. Astrocytes regulate NSC proliferation via secreting growth factors (Shetty, Hattiangady, & Shetty, 2005), but it is unclear whether ferritin from astrocytes regulates NSC proliferation and other NSC behaviors, such as self-renewal and differentiation. Based on our findings, it is feasible to regulate the self-renewal and differentiation of NSCs indirectly through niche cells, which would help to reduce the risk of directly manipulating NSCs to treat neural diseases.

Ferritin and iron

Our results show that ferritin generated outside the brain was not detected in the CNS and vice versa (data not shown), suggesting ferritin can hardly cross the BBB glia, possibly because ferritin is too large to permeate. In this way, BBB glia separates the labile systemic iron from local iron inside the brain to guarantee the normal brain development, as the neural cells, including NBs, require a stable iron level for continuous energy generation during neurogenesis.

Although the dominant function of ferritin is iron storage in mammal, increasing evidence suggests that ferritin also can transport iron. H-ferritin expression in astrocytes is necessary for proper oligodendrocyte development and myelination (Cheli et al., 2021), which implies H-ferritin probably transport iron from astrocytes to oligodendrocytes for myelination. In mice, ferritin heavy chain is secreted by oligodendrocytes via extracellular vesicles (Mukherjee et al., 2020), which possibly endows ferritin with the function of iron transport. Consistently, previous results showed that ferritin can deliver iron across the cultured BBB (Chiou et al., 2019; Fisher et al., 2007). Our results emphasize the critical role of ferritin in iron transport in the CNS. Future studies would be interesting to investigate whether ferritin is able to transport iron in the mammalian brain.

Ferritin specifically targets on the tumor cells, which has been applied to tumor visualization and targeted drug delivery (Fan et al., 2012; Fan et al., 2018). Our study shows that the block of

ferritin or iron can inhibit tumor effectively, which offers an explanation that ferritin targets on tumor is to transport iron for maintaining the cell proliferation, highlighting a potential target for tumor suppression. In consideration of the role of ferritin in normal tissue, such as antioxidant defense function for neurons (Mukherjee et al., 2020), entire block of ferritin for suppressing tumor probably bring neurological disorder. Therefore, we should target on ferritin specifically in tumor to suppress tumor growth.

Iron is an essential component for Fe-S clusters which participate in TCA and OxPhos, providing energy required for self-renewal and proliferation of NBs. Previous study claimed that OxPhos is required for NB proliferation (van den Ameele & Brand, 2019). However, another research observed that OxPhos is dispensable in type II NBs (Bonnay et al., 2020). Our data imply that energy deficiency in NBs caused by iron shortage leads to NB loss and low proliferation possibly through simultaneous disruption of TCA and OxPhos. Consistently, iron-loaded ferritin nanoparticles can be used to improve the self-renewal ability and differentiation potential of human NSCs in vitro (Lee, Yang, Cho, & Cho, 2018). Additionally, previous study has shown that iron-loaded ferritin can promote the proliferation of cultured cell from *Drosophila* (Li, 2010). Furthermore, iron depletion was reported to suppress human cancer cell growth at G1/S by inducing cyclin D1 proteolysis (Nurtjahja-Tjendraputra, Fu, Phang, & Richardson, 2007). These studies suggest that iron, as a necessary microelement for energy production, is essential to NSC maintenance and proliferation.

Bicellular iron homeostasis

Iron homeostasis can be regulated systemically by the liver-derived hormone hepcidin and the iron exporter ferroportin, and it is also regulated cellularly by the IRP/IRE system (Hentze, Muckenthaler, Galy, & Camaschella, 2010). Here we propose a bicellular iron homeostasis between NB and glial niche cell, which is distinct from classic cellular and systemic iron homeostasis. The bicellular iron homeostasis requires an elaborate mechanism to guarantee normal neurogenesis.

In a proliferative state, NBs receive iron from glial cells via ferritin to fulfill the energy requirements for proliferation and self-renewal. Therefore, the iron required by NBs is mainly stored in the ferritin of glial cells and allocated as needed. The bicellular iron homeostasis mechanism makes glial cells the main pool for ferritin production, relieving NBs from the need to produce ferritin and transferring the potential risk of iron overload-induced oxidative stress to glial cells. Furthermore, glial cells can subsequently clear oxidative stress through lipid droplets (Bailey et al., 2015), ensuring normal NB function during neural development. It is intriguing to explore whether bicellular iron homeostasis exists in other stem cells and their niches.

When normal NBs are converted into immortal tumor NBs, becoming highly proliferative, they need more nutrients including iron (Bonnay et al., 2020; van den Ameele & Brand, 2019). In response, more ferritin is generated to transport iron from the glial cells to NBs. However, it is unclear how NBs communicate with glial cells to determine the level of ferritin production. It's interesting to identify the specific cues from NBs that regulate the level of ferritin in future studies. In addition, iron distribution in *Drosophila* brain is not observed due to low iron concentration and technical limitations in iron detection, which results in a lack of direct evidence for iron trafficking via ferritin.

Figure legends

Figure 1. Ferritin in glia is required for NB maintenance and proliferation

(A) NB number and proliferation rate after *Fer1HCH* or *Fer2LCH* RNAi in glia.

(B) Quantification of NB number in CB (A).

(C) Quantification of NB proliferation rate in CB (A).

(D and E) RT-PCR analysis of Fer1HCH and Fer2LCH mRNA levels (D) and normalized quantification (E) after glial ferritin knockdown.

(Fand H) Western blot of Fer1HCH (F) and Fer2LCH (H) after ferritin knockdown in glia. Tubulin was used as a loading control.

(G and I) Quantification of normalized Fer1HCH intensity in (G) and Fer2LCH intensity in (I).

(J) Rescue of NB number and proliferation when simultaneously overexpressing RNAi-resistant *Fer1HCH* and *Fer1HCH RNAi* (or *Fer2LCH* and *Fer2LCH RNAi*) in glia.

(K and L) Quantification of NB number and proliferation rate in (J).

(B, n=11; C, n=10; E, G and I, n=3; K, n=8,8,9,7,9; L, n=9,8,8,7,12; ns, not significant; *: $p<0.05$; **: $p<0.01$; ***: $p<0.001$; ****: $p<0.0001$; Dpn, NB nuclei, red; PH3, green; DAPI, nuclei, blue).

Figure 1-figure supplement 1. Glial ferritin knockdown leads to low NB proliferation and number

(A) Quantification of NB number in VNC.

(B) Quantification of NB proliferation rate in VNC.

(C) EdU incorporation in CNS after knocking down glial ferritin.

(D) Knocking down *Fer2LCH* by *nrv2-GAL4* led to similar but weaker phenotype in brain in comparison with pan-glial ferritin knockdown.

(A, n=11; B, n=10; ****: $p<0.0001$)

Figure 1-figure supplement 2. Ferritin knockdown in different glial subpopulations did not induce any discernible phenotype

(A) Knocking down ferritin genes in subperineurial glia, perineurial glia, ensheathing glia and astrocyte-like glia, respectively

Figure 1-figure supplement 3. Verify the phenotype induced by glial ferritin knockdown using different manipulations

(A) NB number and proliferation in other RNAi lines targeting on ferritin.

(B) Rescue of NB number in VNC when simultaneously overexpressed RNAi-resistant Fer1HCH and Fer1HCH RNAi (or Fer2LCH and Fer2LCH RNAi) in glia.

(C) Rescue of NB proliferation rate in VNC when simultaneously overexpressed RNAi-resistant *Fer1HCH* and *Fer1HCH RNAi* (or *Fer2LCH* and *Fer2LCH RNAi*) in glia.

(D) NB number and proliferation in $Fer1HCH^{DN}$.

(B, n=8,7,9,7,8; C, n=9,8,8,7,12; ****: $p<0.0001$)

Figure 2. Ferritin is produced mainly in glial cells in the *Drosophila* CNS and secreted into NBs through a vesicle dependent pathway

(A) The pattern of DsRed Stinger driven by *Fer1HCH/Fer2LCH-GAL4* in CNS.

(A') The magnification of (A).

(B) The distribution of ferritin labeled by $Fer1HCH^{G188}$ in CNS of control and glial ferritin knockdown.

(B') The magnification of left panel in (B).

(C) Overexpressed ferritin tagged with GFP and mCherry in glia secreted into NBs.
(D) The distribution of *Fer1HCH*^{G188} when blocking glial vesicular trafficking via overexpressing dominant-negative dynamin.
(D') The magnification of (D).
(E) Quantification of (D), GFP signal in NBs when overexpressing *shi* ^{ts} in glia.
(All white circles indicate NB position and white arrows point glial cell; E, n=50, 48; **: p<0.01)

Figure 2-figure supplement 1. *Fer2LCH-GAL4* was used to validate the pattern of *Fer1HCH/Fer2LCH-GAL4*

(A) Most DsRed driven by *Fer2LCH-GAL4* was colocalized with glial marker Repo.

Figure 3. Glial ferritin defects lead to iron deficiency in NBs

(A) The conditions of brain development in *Drosophila* with feeding iron chelator BPS or supplementary iron FAC.
(B) Iron depletion by adding DFP to food exacerbated the phenotype of NB loss induced by glial ferritin knockdown.
(C) Quantification of NB number in (B).
(D) Zip13 in CNS is produced mainly by glial cells, but not NBs.
(D') The magnification of (D). (All white circles indicate NB position and white arrows point glial cells)
(E) Brain defects in *Zip13* knockdown or double knockdown of *Zip13* and *Fer2LCH*.
(F and G) Quantification of NB number and proliferation rate in (E).
(H) Iron supplement can rescue the NB proliferation in *Zip13 RNAi* driven by *repo-GAL4*.
(I) Quantification of NB proliferation in (H).
(C, n=6; F, n=6,10,11,8; G, n=13,10,10,5; I, n=8; ns, not significant; *: p<0.05; **: p<0.01; ****: p<0.0001)

Figure 3-figure supplement 1. Brain defects induced by glial ferritin knockdown were caused by iron deficiency

(A) Test the feeding behavior via adding Brilliant Blue to normal food or BPS food.
(B) Iron deficiency by blocking iron absorption in gut also induced similar brain defects caused by BPS addition.
(C) Quantification of NB number in (B).
(D) Quantification of NB proliferation in (B).
(E) Brain development of glial ferritin knockdown after feeding FAC.
(F) The ratio of brain with NB loss after adding FAC.
(G) NB number and proliferation of *Zip13* mutant.
(H and I) Quantification of NB number and proliferation rate in (G).
(C, n=10; D, n=5; F, n=3; H, n=10,9; I, n=9,8; *: p<0.05; **: p<0.01; ***: p<0.001; ****: p<0.0001)

Figure 3-figure supplement 2. ROS accumulates in CNS after glial ferritin knockdown, but inhibiting ROS cannot restore NB number and proliferation

(A) ROS level marked by Gstd-GFP after knocking down ferritin in glia.
(B) Quantification of ROS level in (A).
(C) Overexpress antioxidant sod1 or cat in glial cells.
(D) Overexpress antioxidant sod1 or cat in NBs.
(E) Mitochondrial morphology by TEM upon glial ferritin knockdown.

(F) Quantification of normal mitochondria in (E). Intact mitochondria with their cristae visible were considered normal.
(G) Western blot of 4-HNE after ferritin knockdown in glia. Actin was used as a loading control.
(H) Quantification of normalized 4-HNE intensity in (G).
(B, n=5,4,5; F, n=23,27,28; H, n=3; ****: $p<0.0001$; ns, not significant)

Figure 3-figure supplement 3. Glial ferritin knockdown does not induce apoptosis in the CNS

(A) Apoptotic signal labeled by Caspase-3 of glial ferritin knockdown.
(B) Quantification of Caspase-3 negative NB ratio.
(C) TUNEL staining of *Fer1HCH RNAi* driven by *repo-GAL4*.
(D) Quantification of TUNEL positive cell per $1x10^5$ μm^2.
(E) P35 overexpression in glia could not rescue brain defects of ferritin knockdown.
(F) Glial morphology was intact when knocking down glial ferritin.
(B, n=5,4,4; D, n=3; ns, not significant)

Figure 4. Glial ferritin defects result in impaired Fe-S cluster activity and ATP production

(A) The determination of cytosolic aconitase activity.
(B) Knockdown of mitochondrial iron-sulfur protein Nfs1 and CIA complex in NBs.
(C) Quantification of NB proliferation in (B).
(D) The schematic diagram of NB sorting procedure.
(E) Venn diagram of downregulated genes after glial ferritin knockdown.
(F) GO enrichment of down-regulated genes in glial ferritin knockdown comparing with control.
(G) KEGG pathway enrichment of down-regulated genes after glial ferritin knockdown.
(H) NAD^+ level was indicated by SoNar.
(I) Quantification of normalized SoNar signal in (H).
(J) The determination of ATP level in CNS.
(K) NB number in glial ferritin knockdown was rescued by Ndi1 overexpression in NBs.
(L) Quantification of NB number in (K).
(A and J, n=3; C, n=5,7,6,6,9; I, n=37,42; L, n=7,7,6,6,7; *: $p<0.05$; **: $p<0.01$; ***: $p<0.001$; ****: $p<0.0001$)

Figure 4-figure supplement 1. Validation of RNA-seq data by qRT-PCR using sorted NB lineages and Ndi1 overexpression

(A) qRT-PCR analysis of *ND-15* and *CG15715* to validate the enrichment result.
(B) Ndi1 overexpression could restore ATP production.
(A and B, n=3; *: $p<0.05$; **: $p<0.01$)

Figure 5. Glial ferritin defects lead to the premature differentiation of NBs

(A) Temporal window of glial ferritin maintaining NBs. The temperature shift of flies with glial ferritin knockdown from the permissive temperature (18℃) to the restrictive temperature (29℃).
(B) Quantification of NB number and proliferation in (A).
(C) Pros staining of knocking down glial ferritin.
(D) Quantification of ratio of $Pros^+Dpn^+$ NBs to Dpn^+ NBs.
(E) Knockdown of *pros* in NBs rescues the NB number.
(F) The ratio of brain with NB loss in (E).
(B, n=6, 5, 6; n=6, 5, 4; D, n=5; F, n=3; *: $p<0.05$; ***: $p<0.001$; ****: $p<0.0001$)

Figure 5-figure supplement 1. NB loss upon glial ferritin knockdown is not due to NB origin

and apoptosis

(A) Temporal window of glial ferritin maintaining NBs. The temperature shift of flies with glial ferritin knockdown from the restrictive temperature (29℃) to the permissive temperature (18℃).

(B) Quantification of NB proliferation in (A).

(C) The CNS of the first-instar larvae with glial ferritin knockdown.

(D) Quantification of NB number and proliferation in (C).

(E) The CNS of the second-instar larvae with glial ferritin knockdown.

(F) Quantification of NB number and proliferation in (E).

(G) P35 overexpression in NBs could not rescue the brain defects induced by glial ferritin knockdown.

(B, n=5; D, n=6; 8,9,8; F, n=11,9,9; 8,9,8; *: $p<0.05$; **: $p<0.01$; ns, not significant)

Figure 5-figure supplement 2. Ndi1 overexpression can restore Pros localization

(A) Pros staining of Ndi1 overexpression upon glial ferritin knockdown.

(B) Quantification of ratio of $Pros^{+}Dpn^{+}$ NBs to Dpn^{+} NBs in (A).

(B, n=6,9; ***: $p<0.001$)

Figure 5-figure supplement 3. Glial ferritin defects do not affect NB reactivation and asymmetric division

(A) aPKC localization in NB after knocking down *Fer2LCH*.

(B) NB size upon glial ferritin knockdown was not changed.

(C) Activation of Insulin signaling could not restore NB number and proliferation.

(D) Quantification of NB proliferation in (B).

(B, n=100; D, n=8, 5; ns, not significant)

Figure 6. Ferritin functions as a potential target for tumor suppression

(A) Knockdown of ferritin in glia could inhibit the tumor induced by *numb RNAi*.

(B) Quantification of larval brain size in (A).

(C) Iron chelator BPS supplemented in the food suppressed brain tumor growth.

(D) Quantification of larval brain size in (C).

(E) Bioluminescence signal in mice with glioma on day 14.

(F) Quantification of bioluminescence signal in (E).

(G) Kaplan-Meier survival curve of mice treated with DFP.

(B, n=6,7,5; D, n=5,6,6; F, n=6,7; G, n=7,6; *: $p<0.05$; **: $p<0.01$ ***: $p<0.001$; ****: $p<0.0001$)

Figure 6-figure supplement 1. Iron chelator inhibits tumor progression in *Drosophila* and mice

(A) Knockdown of ferritin in glia could inhibit the tumor induced by *brat RNAi*.

(B) Quantification of larval brain size in (A).

(C) Iron chelator BPS suppressed brain tumor growth of *brat RNAi*.

(D) Quantification of larval brain size in (C).

(E) The appearance and HE staining of brains in mice with DFP injection on day 7, 14 and 21. Scar bar: 1000 μm.

(F and G) Quantification of HE staining in murine brains on day 14 (B) and 21 (C).

(B, n=10,7; D, n=8,6; F, n=6; G, n=9,8; ***: $p<0.001$; ****: $p<0.0001$.)

Figure 7. The level of ferritin is controlled by NB proliferation

(A) Fer1HCH subunit level in *Drosophila* CNS after manipulating proliferation.

(B) Fer2LCH subunit level in *Drosophila* CNS after manipulating proliferation.

(C) Quantification of Fer1HCH level in (A).
(D) Quantification of Fer2LCH level in (B).
(E) The model of glial ferritin regulating NBs.
(C and D, n=3; ns, not significant; *: $p<0.05$; **: $p<0.01$; ***: $p<0.001$)

Materials and methods

Fly Genetics

Fly strains were bred on yeast-containing medium at constant temperature 25℃ in 12h light/dark cycle unless otherwise stated. UAS-Fer1HCH-RNAi (THU5585) and UAS-Fer2LCH-RNAi (TH01861.N) were used for most experiments except Figure1-figure supplement 2A (BDSC: 60000, VDRC: 14491 and VDRC: 12925) and Figure3-figure supplement 3E (VDRC: 14491). *UAS-Fer1HCH*, *UAS-Fer2LCH*, *lexAop-Fer1HCH-RNAi* and *lexAop-Fer2LCH-RNAi* were generated in this paper. *GstD1-GFP was* from Fisun Hamaratoglu. *repo-lexA* was from Margaret S Ho. *UAS-Ndi1 and UAS-SoNar* were from Juergen A. Knoblich. *Insc-GAL4* (BDSC:8751) was from Yan Song. *UAS-RedStinger* was BDSC:8546. *UAS-Fer1HCH::GFP;UAS-Fer2LCH::mCherry* was from Fanis Missirlis. *Fer1HCH*^{G188} was from Bing Zhou. Other fly lines used in this study were bought from Bloomington Drosophila Stock Center, Tsinghua Fly Center, Vienna Drosophila Resource Center, and Drosophila Genetic Resource Center (Table 2 and 3 in supplementary material).

Screen

200 RNAi lines were screened in this study. These genes were related to classical signaling pathway, high expression in glial cells or secretory protein. *UAS-RNAi* lines were crossed with *repo-Gal4*, then the third-instar larvae of F1 were dissected to harvest brains. Brains were performed immunostaining with Dpn and PH3. Finally, brains were observed in Confocal Microscope.

Mouse husbandry

All mouse experiments were performed under the guidelines of the Institutional Animal Care and Use Committee at Southeast University. Mice were maintained in a barrier facility, at 25℃, on a regular 12h light and 12h dark cycle.

DNA and Plasmids

For generating RNAi-resistant UAS-Fer1HCH and UAS-Fer2LCH constructs used for transgenic fly lines, Fer1HCH cDNA (PA type) and Fer2LCH cDNA (PA type) with silent mutations in the region targeted by siRNA were inserted into pUAST plasmids, respectively. The cDNA with silent mutations was synthesized by Sangon Biotech (Shanghai) Co., Ltd. To generate transgenic fly lines of lexAop-Fer1HCH-RNAi and lexAop-Fer2LCH-RNAi, the shRNA sequences targeted on Fer1HCH and Fer2LCH were generated by PCR amplification of UAS-Fer1HCH-RNAi (TH01861.N) and UAS-Fer2LCH-RNAi (THU5585) DNA using primers (5'-ACGGAGCGACAATTCAATTCA-3'/5'-TGATGCCTACCTGATGCCAA-3'), respectively. The fragments were digested by EcoRI and XbaI, then ligated into lexAop vectors. The constructs were verified by sequencing.

Immunostaining and Antibodies

Larval brains were dissected in PBS (1×), fixed in 4% paraformaldehyde/PBS for 20 min and washed 3 times with 0.3% PBST (Triton X-100). Then the brains blocked in 1% BSA for 1h at room temperature. Finally, these brains were incubated with antibodies overnight at 4℃. Primary antibodies: Guinea pig anti-Dpn (1:1000, gift from Juergen A. Knoblich), rabbit anti-PH3 (1/100, CST, 9701), rat anti-Mira (1/1000, abcam, ab197788), mouse anti-Repo (1/100, DSHB, 8D12), rabbit anti-GFP (1/1000, Torrey Pines Biologies, TP401), rabbit anti-Caspase3 (1/100, CST, 9661), mouse anti-Pros (1/20, DSHB), mouse anti-aPKC (1/50, Santa Cruz, Sc-17781).

To detect primary antibodies, the following Alexa-Flour conjugated second antibodies from Invitrogen were used: goat anti-rat Alexa 555 (1/100, A21434), goat anti-guinea pig Alexa 555 (1/100, A21435), donkey anti-rabbit Alexa 488 (1/100, A21206), donkey anti-rat Alexa 488 (1/100, A21208), donkey anti-mouse Alexa 488 (1/100, A21202), goat anti-rat Alexa 633 (1/100, A21094), donkey anti-mouse Alexa 647 (1/100, A31571). All immunostaining images were captured using an LSM700 or an LSM900 (Zeiss) confocal microscope.

EdU and TUNEL

Dissected freshly brains were incubated in EdU solution for about 30 min to incorporate EdU, then fixed and permeabilized referring to the steps from immunostaining. EdU was detected by Click-iT EdU Alexa Fluor 555 Imaging Kit according to the instructions. TUNEL detection was determined using kit based on the manufacturer's instructions.

RNA Isolation, Semiquantitative RT-PCR, and Quantitative Real-time PCR

Total RNA was extracted from larval brains by TRIzol reagent. cDNA was reverse-transcribed from total RNA using kit. Semiquantitative RT-PCR was performed using the specific primers to amplify the targeted gene segment. Quantitative Real-time PCR was performed on LightCycler 96 (Bio-Rad) using qPCR SuperMix (TransGen Biotech). Following primers were used:

rp49 F: GCACCAAGCACTTCATCC
rp49 R: CGATCTCGCCGCAGTAAA
Fer1HCH F: ATGGTGAAACTAATTGCTAGC
Fer1HCH R: TCAGATCGCTGACTCCCTC
Fer2LCH F: GCATGCTCTACGTCAGCCT
Fer2LCH R: TTACTGCTTCTGCAGATACTC
ND15 F: ATGTCGCTTACCCCCTTTCTACG
ND15 R: CTAGTAGGCATCAACGCGTGG
CG15715 F: ATGGCACGTGGACACCAG
CG15715 R: TCAGACCTCCTTCAGCTCCTCG

Western blot and Antibodies

Brains were dissected in PBS, then homogenized in the RIPA buffer with SDS. Homogenate was centrifuged at 12000 rpm for 5 min at 4℃ three times and boiled for 10 min. The protein was

separated on 15% SDS-PAGE and transferred to nitrocellulose membranes. The membranes were blocked in 5% milk and incubated overnight at 4℃ with antibodies. The blots were detected using Tanon 5200. Primary antibodies used: rabbit anti-Fer1HCH (1/500, this study), rabbit anti-Fer2LCH (1/500, this study), mouse anti-tubulin (1/1000, abcam, ab7291), mouse anti-Repo (1/200, DSHB, 8D12), rabbit anti-4-HNE (1/1000, abcam, ab46545). Rabbit polyclonal antibodies were generated against recombinant proteins His-Fer1HCH or His-Fer2LCH. In brief, the aa 23–200 of Fer1HCH (PA type) or aa 41–227 of Fer2LCH (PA type), contained by different Fer1HCH or Fer2LCH cDNA isoforms, was synthesized and cloned into pET28a vector respectively. The recombinant proteins were expressed in *E. coli*, extracted, and injected into rabbit for generating the antibodies (Abclonal Biotech.). Then the antibodies were affinity-purified and applied in western blot.

Temperature Shift

GAL80^{ts} was introduced into this system to control the function of GAL4 according to the temperature for determining the temporal window during which ferritin functions to maintain NBs. The eggs of *tubulin-GAL80^{ts}; repo-gal4* crossing with *UAS-Fer1HCH RNAi* or *UAS-Fer2LCH RNAi* were collected, and cultured at 18℃ (permissive temperature for GAL80^{ts}) before hatching, then transferred to 29℃ (restrictive temperature for GAL80^{ts}) after hatching, or vice versa until third-instar larval stage. Then brains were observed and analyzed.

Culture Medium

Supplemented iron salt and iron chelators (1×) in *Drosophila* food were used as follows: 5 mM ferric ammonium citrate (FAC) (sigma), 0.1 mM bathophenanthrolinedisulfonic acid disodium (BPS) (sigma), 2.5 mM deferiprone (DFP) (sigma).

Cell Dissociation and FACS

NB lineages were labeled with DsRed drived by *Insc-GAL4*. These cells were dissociated and sorted according to previous protocol (Harzer et al., 2013). Briefly, brains were dissected in Schneider's medium and transferred into Rinaldini's solution. Then Rinaldini's solution was removed, and dissociation solution was added to the brains to incubate at 30℃ for 1h. After washing these brains twice in Rinaldini's solution, the brains were disrupted in PBS. Finally, NB lineages were sorted by flow cytometer (Beckman) based on the red signal.

RNA Sequencing and Data Processing

Smart-Seq2 libraries preparation

The sorted NBs were collected into microtubes with ribonuclease inhibitor and lysis component. An Oligo-dT primer was added to the reverse transcription reaction for first-strand cDNA synthesis, followed by PCR amplification to enrich the cDNA and magbeads purification to clean up the production. Then qualified cDNA was sheared randomly by ultrasonic waves for Illumina library preparation protocol including DNA fragmentation, end repair, 3' ends A-tailing, adapter

ligation, PCR amplification, and library validation. After library preparation, PerkinElmer LabChip®GX Touch and Step OnePlus™ Real-Time PCR System were introduced for library quality inspection. Qualified libraries were then loaded on Illumina Hiseq platform for PE150 sequencing (Annoroad Gene Technology Co., Ltd).

Quantification and Differential Expression Analysis

The reads containing adapter sequences, low-quality reads or undetermined bases were removed from raw data using fastp program. The clean reads were aligned to the reference genome of *Drosophila melanogaster* using HISAT2 (v2.1.0). The Ensembl database was chosen as the annotation reference. The gene expression was calculated as Fragments Per Kilobase Million mapped reads (FPKM). The differential expression of genes was analyzed with DEGSeq package. The criterion of |log2 (fold-change)| ≥1 and p-value < 0.05 was used to identify differentially expressed genes.

GO and KEGG Pathway Enrichment

Gene Ontology (GO) enrichment analysis and Kyoto Encyclopedia of Genes and Genomes (KEGG) pathway analysis were performed to investigate the function of differentially expressed genes. GO analysis was used to explore the function of genes, such as biological process, cellular component, and molecular function. KEGG analysis focused on finding and analyzing interactions in biological systems, such as signal transduction and disease pathways. Only the gene sets with p-value < 0.05 were significantly enriched.

Aconitase Activity Assay

Protein was extracted with assay buffer from Aconitase Activity Assay Kit (sigma, MAK051). The concentration of protein was determined by Pierce™ Rapid Gold BCA Protein Assay Kit (Thermo Fisher, A53225). Aconitase was measured according to the Aconitase Activity Assay Kit.

TEM observation and analysis

TEM samples were prepared by standard procedures (Gan, Geng, Zhang, Mou, & Xie, 2020). In brief, brains from third instar larvae upon WT and glial ferritin knockdown were dissected in fresh PBS and fixed at 4°C overnight in a mixture of 2% glutaraldehyde and 2% formaldehyde in 0.1 M sodium cacodylate buffer (pH 7.4), followed by several rinses with cacodylate buffer. The samples were then postfixed for 2 h with 1% OsO_4 in cacodylate buffer and rinsed twice with distilled water. The preparations were stained for 2 h with 2% saturated uranyl acetate in distilled water and rinsed twice with distilled water. The specimens were dehydrated in an ethanol series, passed through propylene oxide two times, and embedded into a sheet in Epon812 (SPI Science). Each slice was 90 nm thick, 30–40 slices were gathered into a group and attached to a grid. Samples were analyzed with Hitachi H-7650 electron microscope operated at 80kV.

Orthotopic Glioma Model and DFP Injection

To establish an orthotopic glioma model (B. Wang et al., 2022), C57BL/6 mice (4-6 weeks) were anesthetized using 2% isoflurane and positioned in a stereotactic instrument. GL261-luc cell

suspension (1×10^5 cells in 3 μL PBS) was injected into the striatum. Specifically, the injection site is at 0.5 mm anterior, 2 mm lateral to the bregma and 3.5 mm below the skull. The injection was done slowly about 10 min.

The mice with glioma were injected intraperitoneally with DFP every 48 h (Eybl, Kotyzova, Kolek, Koutensky, & Nielsen, 2002). DFP was dissolved in saline (0.9% NaCl) to 10 mg/ml. The doses of injection in mice were 150 mg/kg using 10 mg/ml DFP. The injection volume was determined based on murine weight.

Bioluminescence Imaging

For tumor imaging, mice were injected with luciferin (150 μg/g) in PBS (S. L. Wang et al., 2019). After 10 min, the mice were imaged using the IVIS Spectrum (PerkinElmer).

HE Staining

At time of sacrifice, mouse brains were removed and fixed in 4 % paraformaldehyde for 24 h. After fixation, brains were immersed in 30 % sucrose and embedded in OCT for cryosectioning. Sections were stained by Hematoxylin and Eosin (HE). Tumor volumes were estimated using Image J.

Quantifications and Statistical Analysis

For quantification of NSCs, Dpn- or Mira-positive NSC of CB or the thoracic VNC at the indicated stage were counted. Mitotic index is the number of PH3-positive cells among Dpn-positive cells. For tumor size in *Drosophila*, the area of CNS was measured by NIH ImageJ. For quantifications of NB size, fluorescence or western blot intensity, NIH ImageJ was used to measure.

All experiments were repeated at least three times. The figure legends showed the number of samples, statistical parameters, and significance. GraphPad Prism 6 was used to perform statistical analyses. For comparisons between two groups, unpaired two-sided Student's t test was employed to assess statistical significance. For comparisons between three of more groups, statistical significance was determined using one-way ANOVA with a Bonferroni test. The log-rank test was used to compare the survival curves of mice. The sample distributions were assumed to be normal and no particular statistical tests were used to check for normality within the samples. Statistical results were presented as means ± SD and p values of less than 0.05 were considered statistically significant. Asterisks indicate critical levels of significance (*: $p<0.05$; **: $p<0.01$; ***: $p<0.001$; ****: $p<0.0001$).

Data availability

RNA-seq data are available at the GEO database, accession number GEO GSE237124 and reviewer token: cnqxqoqonzapjst

Any additional information required to reanalyze the data reported in this paper is available from the lead contact upon request.

Acknowledgments

We are grateful to Drs. Bing Zhou, Margaret S Ho, Juergen A. Knoblich, Fanis Missirlis, Fisun Hamaratoglu, Yan Song, Andrea H. Brand; Bloomington Drosophila Stock Center (Indiana

University, Bloomington, Indiana), the Drosophila Genetic Resource Center (Kyoto Institute of Technology, Kyoto, Japan), the Vienna Drosophila RNAi Center (Vienna, Austria), and Tsinghua Fly Center (Tsinghua University) for fly stocks and reagents. We thank Dr. Bing Zhou for the useful advice on this study. We thank Drs. Junhua Geng, and Mingdao Mu for comments on the manuscript. This study was supported by the National Natural Science Foundation of China (31970675).

Funding

National Natural Science Foundation of China (grant no. 32100784, grant recipient, Menglong Rui; grant no. 31970675, grant recipient, Su Wang)

Author contributions

Zhixin Ma, Resources, Data curation, Formal analysis, Validation, Investigation, Methodology, Writing - original draft; Wenshu Wang, Resources, Formal analysis, Investigation, Methodology; Xiaojing Yang, Formal analysis, Methodology; Menglong Rui, Writing - review and editing; Su Wang, Conceptualization, Resources, Supervision, Funding acquisition, Investigation, Project administration, Writing - review and editing.

Competing interests

The authors declare no competing interests.

References

Andrews, N. C. (2005). Molecular control of iron metabolism. *Best Pract Res Clin Haematol, 18*(2), 159-169. doi:10.1016/j.beha.2004.10.004

Arosio, P., Ingrassia, R., & Cavadini, P. (2009). Ferritins: A family of molecules for iron storage, antioxidation and more. *Biochimica Et Biophysica Acta-General Subjects, 1790*(7), 589-599. doi:10.1016/j.bbagen.2008.09.004

Bailey, A. P., Koster, G., Guillermier, C., Hirst, E. M., MacRae, J. I., Lechene, C. P., . . . Gould, A. P. (2015). Antioxidant Role for Lipid Droplets in a Stem Cell Niche of Drosophila. *Cell, 163*(2), 340-353. doi:10.1016/j.cell.2015.09.020

Bjornsson, C. S., Apostolopoulou, M., Tian, Y., & Temple, S. (2015). It takes a village: constructing the neurogenic niche. *Dev Cell, 32*(4), 435-446. doi:10.1016/j.devcel.2015.01.010

Bonnay, F., Veloso, A., Steinmann, V., Kocher, T., Abdusselamoglu, M. D., Bajaj, S., . . . Knoblich, J. A. (2020). Oxidative Metabolism Drives Immortalization of Neural Stem Cells during Tumorigenesis. *Cell, 182*(6), 1490-1507 e1419. doi:10.1016/j.cell.2020.07.039

Bowman, S. K., Rolland, V., Betschinger, J., Kinsey, K. A., Emery, G., & Knoblich, J. A. (2008). The tumor suppressors brat and numb regulate transit-amplifying neuroblast lineages in Drosophila. *Developmental Cell, 14*(4), 535-546. doi:10.1016/j.devcel.2008.03.004

Cabernard, C., & Doe, C. Q. (2009). Apical/Basal Spindle Orientation Is Required for Neuroblast Homeostasis and Neuronal Differentiation in Drosophila. *Developmental Cell, 17*(1), 134-141. doi:10.1016/j.devcel.2009.06.009

Cheli, V. T., González, D. A. S., Wan, Q. C., Denaroso, G., Wan, R. S., Rosenblum, S. L., & Paez, P. M. (2021). H-ferritin expression in astrocytes is necessary for proper oligodendrocyte development and myelination. *Glia, 69*(12), 2981-2998. doi:10.1002/glia.24083

Chell, J. M., & Brand, A. H. (2010). Nutrition-responsive glia control exit of neural stem cells from quiescence. *Cell, 143*(7), 1161-1173. doi:10.1016/j.cell.2010.12.007

Chiou, B., Neal, E. H., Bowman, A. B., Lippmann, E. S., Simpson, I. A., & Connor, J. R. (2019). Endothelial cells are critical regulators of iron transport in a model of the human blood-brain barrier. *J Cereb Blood Flow Metab, 39*(11), 2117-2131. doi:10.1177/0271678X18783372

Choksi, S. P., Southall, T. D., Bossing, T., Edoff, K., de Wit, E., Fischer, B. E., . . . Brand, A. H. (2006). Prospero acts as a binary switch between self-renewal and differentiation in

926 Drosophila neural stem cells. *Developmental Cell, 11*(6), 775-789.
927 doi:10.1016/j.devcel.2006.09.015
928 Eybl, V., Kotyzova, D., Kolek, M., Koutensky, J., & Nielsen, P. (2002). The influence of
929 deferiprone (L1) and deferoxamine on iron and essential element tissue level and
930 parameters of oxidative status in dietary iron-loaded mice. *Toxicology Letters,*
931 *128*(1-3), 169-175. doi:Pii S0378-4274(01)00541-0
932 Doi 10.1016/S0378-4274(01)00541-0
933 Fan, K., Cao, C., Pan, Y., Lu, D., Yang, D., Feng, J., . . . Yan, X. (2012). Magnetoferritin
934 nanoparticles for targeting and visualizing tumour tissues. *Nat Nanotechnol, 7*(7),
935 459-464. doi:10.1038/nnano.2012.90
936 Fan, K., Jia, X., Zhou, M., Wang, K., Conde, J., He, J., . . . Yan, X. (2018). Ferritin Nanocarrier
937 Traverses the Blood Brain Barrier and Kills Glioma. *ACS Nano, 12*(5), 4105-4115.
938 doi:10.1021/acsnano.7b06969
939 Fisher, J., Devraj, K., Ingram, J., Slagle-Webb, B., Madhankumar, A. B., Liu, X., . . . Connor, J.
940 R. (2007). Ferritin: a novel mechanism for delivery of iron to the brain and other
941 organs. *Am J Physiol Cell Physiol, 293*(2), C641-649. doi:10.1152/ajpcell.00599.2006
942 Fretham, S. J., Carlson, E. S., & Georgieff, M. K. (2011). The role of iron in learning and
943 memory. *Adv Nutr, 2*(2), 112-121. doi:10.3945/an.110.000190
944 Gan, G. M., Geng, J. H., Zhang, C. C., Mou, Y., & Xie, W. (2020). Neurexin and Neuroligins
945 Maintain the Balance of Ghost and Satellite Boutons at the Drosophila Neuromuscular
946 Junction. *Frontiers in Neuroanatomy, 14*. doi:ARTN 19
947 10.3389/fnana.2020.00019

948 Haile, D. J., Rouault, T. A., Harford, J. B., Kennedy, M. C., Blondin, G. A., Beinert, H., &
949 Klausner, R. D. (1992). Cellular regulation of the iron-responsive element binding
950 protein: disassembly of the cubane iron-sulfur cluster results in high-affinity RNA
951 binding. *Proc Natl Acad Sci U S A, 89*(24), 11735-11739.
952 doi:10.1073/pnas.89.24.11735
953 Hartenstein, V. (2011). Morphological Diversity and Development of Glia in Drosophila. *Glia,*
954 *59*(9), 1237-1252. doi:10.1002/glia.21162
955 Harzer, H., Berger, C., Conder, R., Schmauss, G., & Knoblich, J. A. (2013). FACS purification
956 of Drosophila larval neuroblasts for next-generation sequencing. *Nat Protoc, 8*(6),
957 1088-1099. doi:10.1038/nprot.2013.062
958 Hentze, M. W., Muckenthaler, M. U., Galy, B., & Camaschella, C. (2010). Two to Tango:
959 Regulation of Mammalian Iron Metabolism. *Cell, 142*(1), 24-38.
960 doi:10.1016/j.cell.2010.06.028
961 Hirschhorn, T., & Stockwell, B. R. (2019). The development of the concept of ferroptosis. *Free*
962 *Radical Biology and Medicine, 133*, 130-143.
963 doi:10.1016/j.freeradbiomed.2018.09.043
964 Ito, K., Urban, J., & Technau, G. M. (1995). Distribution, Classification, and Development of
965 Drosophila Glial-Cells in the Late Embryonic and Early Larval Ventral Nerve Cord.
966 *Rouxs Archives of Developmental Biology, 204*(5), 284-307. doi:Doi
967 10.1007/Bf02179499
968 Knovich, M. A., Storey, J. A., Coffman, L. G., Torti, S. V., & Torti, F. M. (2009). Ferritin for the
969 clinician. *Blood Rev, 23*(3), 95-104. doi:10.1016/j.blre.2008.08.001

970 Kosmidis, S., Botella, J. A., Mandilaras, K., Schneuwly, S., Skoulakis, E. M. C., Rouault, T. A.,
971 & Missirlis, F. (2011). Ferritin overexpression in
972 glia leads to iron deposition in the optic lobes and late-onset behavioral defects. *Neurobiology*
973 *of Disease, 43*(1), 213-219. doi:10.1016/j.nbd.2011.03.013
974 Lee, J. S., Yang, K., Cho, A. N., & Cho, S. W. (2018). Ferritin nanoparticles for improved
975 self-renewal and differentiation of human neural stem cells. *Biomater Res, 22*, 5.
976 doi:10.1186/s40824-018-0117-y
977 Li, S. (2010). Identification of iron-loaded ferritin as an essential mitogen for cell proliferation
978 and postembryonic development in Drosophila. *Cell Res, 20*(10), 1148-1157.
979 doi:10.1038/cr.2010.102
980 Lind, M. I., Ekengren, S., Melefors, O., & Soderhall, K. (1998). Drosophila ferritin mRNA:
981 alternative RNA splicing regulates the presence of the iron-responsive element. *FEBS*
982 *Lett, 436*(3), 476-482. doi:10.1016/s0014-5793(98)01186-7
983 Lozoff, B., Beard, J., Connor, J., Barbara, F., Georgieff, M., & Schallert, T. (2006). Long-lasting
984 neural and behavioral effects of iron deficiency in infancy. *Nutr Rev, 64*(5 Pt 2),
985 S34-43; discussion S72-91. doi:10.1301/nr.2006.may.s34-s43
986 Ly, P. T., Tan, Y. S., Koe, C. T., Zhang, Y., Xie, G., Endow, S., . . . Wang, H. (2019).
987 CRL4Mahj E3 ubiquitin ligase promotes neural stem cell reactivation. *PLoS Biol, 17*(6),
988 e3000276. doi:10.1371/journal.pbio.3000276
989 Missirlis, F., Kosmidis, S., Brody, T., Mavrakis, M., Holmberg, S., Odenwald, W. F., . . .
990 Rouault, T. A. (2007). Homeostatic mechanisms for iron storage revealed by genetic
991 manipulations and live imaging of Drosophila ferritin. *Genetics, 177*(1), 89-100.

992 doi:10.1534/genetics.107.075150

993 Moller, H. E., Bossoni, L., Connor, J. R., Crichton, R. R., Does, M. D., Ward, R. J., . . . Ronen, I.
994 (2019). Iron, Myelin, and the Brain: Neuroimaging Meets Neurobiology. *Trends*
995 *Neurosci, 42*(6), 384-401. doi:10.1016/j.tins.2019.03.009

996 Mukherjee, C., Kling, T., Russo, B., Miebach, K., Kess, E., Schifferer, M., . . . Simons, M.
997 (2020). Oligodendrocytes Provide Antioxidant Defense Function for Neurons by
998 Secreting Ferritin Heavy Chain. *Cell Metab, 32*(2), 259-272 e210.
999 doi:10.1016/j.cmet.2020.05.019

1000 Mumbauer, S., Pascual, J., Kolotuev, I., & Hamaratoglu, F. (2019). Ferritin heavy chain
1001 protects the developing wing from reactive oxygen species and ferroptosis. *PLoS*
1002 *Genet, 15*(9), e1008396. doi:10.1371/journal.pgen.1008396

1003 Navarro, J. A., Botella, J. A., Metzendorf, C., Lind, M. I., & Schneuwly, S. (2015). Mitoferrin
1004 modulates iron toxicity in a Drosophila model of Friedreich's ataxia. *Free Radical*
1005 *Biology and Medicine, 85*, 71-82. doi:10.1016/j.freeradbiomed.2015.03.014

1006 Nichol, H., Law, J. H., & Winzerling, J. J. (2002). Iron metabolism in insects. *Annual Review of*
1007 *Entomology, 47*, 535-559. doi:DOI 10.1146/annurev.ento.47.091201.145237

1008 Nurtjahja-Tjendraputra, E., Fu, D., Phang, J. M., & Richardson, D. R. (2007). Iron chelation
1009 regulates cyclin D1 expression via the proteasome: a link to iron deficiency-mediated
1010 growth suppression. *Blood, 109*(9), 4045-4054. doi:10.1182/blood-2006-10-047753

1011 Pereanu, W., Shy, D., & Hartenstein, V. (2005). Morphogenesis and proliferation of the larval
1012 brain glia in Drosophila. *Developmental Biology, 283*(1), 191-203.
1013 doi:10.1016/j.ydbio.2005.04.024

1014 Pham, D. Q., & Winzerling, J. J. (2010). Insect ferritins: Typical or atypical? *Biochim Biophys*
1015 *Acta, 1800*(8), 824-833. doi:10.1016/j.bbagen.2010.03.004
1016 Read, R. D. (2018). Pvr receptor tyrosine kinase signaling promotes post-embryonic
1017 morphogenesis, and survival of glia and neural progenitor cells in Drosophila.
1018 *Development, 145*(23). doi:10.1242/dev.164285
1019 Reichardt, I., Bonnay, F., Steinmann, V., Loedige, I., Burkard, T. R., Meister, G., & Knoblich, J.
1020 A. (2018). The tumor suppressor Brat controls neuronal stem cell lineages by
1021 inhibiting Deadpan and Zelda. *EMBO Rep, 19*(1), 102-117.
1022 doi:10.15252/embr.201744188
1023 Rice, D., & Barone, S., Jr. (2000). Critical periods of vulnerability for the developing nervous
1024 system: evidence from humans and animal models. *Environ Health Perspect, 108*
1025 *Suppl 3*, 511-533. doi:10.1289/ehp.00108s3511
1026 Sawicki, R., Singh, S. P., Mondal, A. K., Benes, H., & Zimniak, P. (2003). Cloning, expression
1027 and biochemical characterization of one Epsilon-class (GST-3) and ten Delta-class
1028 (GST-1) glutathione S-transferases from
1029 , and identification of additional nine members of the Epsilon class. *Biochemical Journal, 370*,
1030 661-669. doi:10.1042/Bj20021287
1031 Shetty, A. K., Hattiangady, B., & Shetty, G. A. (2005). Stem/progenitor cell proliferation factors
1032 FGF-2, IGF-1, and VEGF exhibit early decline during the course of aging in the
1033 hippocampus: role of astrocytes. *Glia, 51*(3), 173-186. doi:10.1002/glia.20187
1034 Soriano, S., Llorens, J. V., Blanco-Sobero, L., Gutiérrez, L., Calap-Quintana, P., Morales, M.
1035 P., . . . Martínez-Sebastián, M. J. (2013). Deferiprone and idebenone rescue frataxin

1036 depletion phenotypes in a
1037 model of Friedreich's ataxia. *Gene, 521*(2), 274-281. doi:10.1016/j.gene.2013.02.049
1038 Sousa-Nunes, R., Yee, L. L., & Gould, A. P. (2011). Fat cells reactivate quiescent neuroblasts
1039 via TOR and glial insulin relays in Drosophila. *Nature, 471*(7339), 508-512.
1040 doi:10.1038/nature09867
1041 Speder, P., & Brand, A. H. (2014). Gap junction proteins in the blood-brain barrier control
1042 nutrient-dependent reactivation of Drosophila neural stem cells. *Dev Cell, 30*(3),
1043 309-321. doi:10.1016/j.devcel.2014.05.021
1044 Speder, P., & Brand, A. H. (2018). Systemic and local cues drive neural stem cell niche
1045 remodelling during neurogenesis in Drosophila. *Elife, 7*. doi:10.7554/eLife.30413
1046 Sykiotis, G. P., & Bohmann, D. (2008). Keap1/Nrf2 signaling regulates oxidative stress
1047 tolerance and lifespan in Drosophila. *Dev Cell, 14*(1), 76-85.
1048 doi:10.1016/j.devcel.2007.12.002
1049 Tang, X., & Zhou, B. (2013). Ferritin is the key to dietary iron absorption and tissue iron
1050 detoxification in Drosophila melanogaster. *FASEB J, 27*(1), 288-298.
1051 doi:10.1096/fj.12-213595
1052 Tanimura, T., Isono, K., Takamura, T., & Shimada, I. (1982). Genetic Dimorphism in the Taste
1053 Sensitivity to Trehalose in Drosophila-Melanogaster. *Journal of Comparative*
1054 *Physiology, 147*(4), 433-437. doi:Doi 10.1007/Bf00612007
1055 Tong, W. H., & Rouault, T. A. (2006). Functions of mitochondrial ISCU and cytosolic ISCU in
1056 mammalian iron-sulfur cluster biogenesis and iron homeostasis. *Cell Metab, 3*(3),
1057 199-210. doi:10.1016/j.cmet.2006.02.003

1058 van den Ameele, J., & Brand, A. H. (2019). Neural stem cell temporal patterning and brain
1059 tumour growth rely on oxidative phosphorylation. *Elife, 8*. doi:10.7554/eLife.47887
1060 Wang, B., Tang, M. P., Yuan, Z. W., Li, Z. Y., Hu, B., Bai, X., . . . Zhang, X. Q. (2022). Targeted
1061 delivery of a STING agonist to brain tumors using bioengineered protein nanoparticles
1062 for enhanced immunotherapy. *Bioactive Materials, 16*, 232-248.
1063 doi:10.1016/j.bioactmat.2022.02.026
1064 Wang, S. L., Yao, F. L., Lu, X. H., Li, Q., Su, Z. P., Lee, J. H., . . . Du, L. Y. (2019).
1065 Temozolomide promotes immune escape of GBM cells via upregulating PD-L1.
1066 *American Journal of Cancer Research, 9*(6), 1161-+. Retrieved from <Go to
1067 ISI>://WOS:000473286300006
1068 Xiao, G., Liu, Z. H., Zhao, M., Wang, H. L., & Zhou, B. (2019). Transferrin 1 Functions in Iron
1069 Trafficking and Genetically Interacts with Ferritin in Drosophila melanogaster. *Cell Rep,*
1070 *26*(3), 748-758 e745. doi:10.1016/j.celrep.2018.12.053
1071 Xiao, G., Wan, Z., Fan, Q., Tang, X., & Zhou, B. (2014). The metal transporter ZIP13 supplies
1072 iron into the secretory pathway in Drosophila melanogaster. *Elife, 3*, e03191.
1073 doi:10.7554/eLife.03191
1074 Zhao, Y. Z., Wang, A. X., Zou, Y. J., Su, N., Loscalzo, J., & Yang, Y. (2016). monitoring of
1075 cellular energy metabolism using SoNar, a highly responsive sensor for NAD
1076 /NADH redox state. *Nature Protocols, 11*(8), 1345-1359. doi:10.1038/nprot.2016.074
1077
1078
1079
1080
1081
1082

AL4 driver	Stock center	Stock number	Expression pattern	Fer1HCH RNAi	Fer2LCH RNAi
repo-GAL4	BDSC	7415	all glia	+++	+++
nrv2-GAL4	BDSC	6799	cortex glia	+	+
mdr65-GAL4	BDSC	50472	subperineurial glia	-	-
moody-GAL4	BDSC	90883	subperineurial glia	-	-
NP6293-GAL4	DGRC	105188	perineurial glia	-	-
alrm-GAL4	BDSC	67032	astrocyte-like glia	-	-
NP6520-GAL4	DGRC	105240	ensheathing glia	-	-

Table 1. The phenotype of ferritin knockdown in different glial subpopulations. BDSC: Bloomington Drosophila Stock Center; DGRC: Drosophila Genetic Resource Center; +++: strong phenotype; ++: weak phenotype; -: no phenotype.

Figure 1

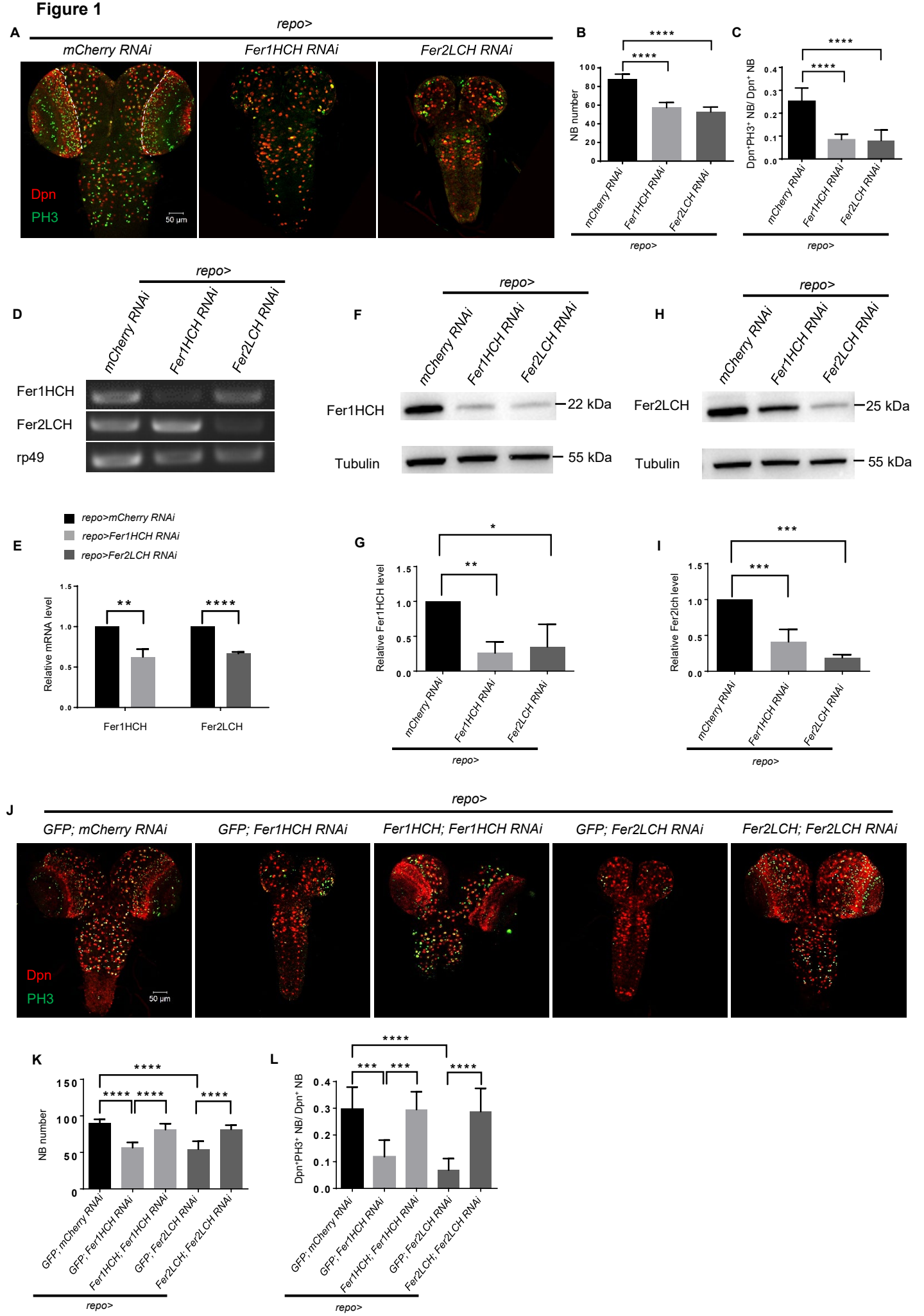
A
repo>
mCherry RNAi
Fer1HCH RNAi
Fer2LCH RNAi
Dpn
PH3
50 μm
B
NB number
mCherry RNAi
Fer1HCH RNAi
Fer2LCH RNAi
repo>
C
Dpn+PH3+ NB/ Dpn+ NB
D
Fer1HCH
Fer2LCH
rp49
E
repo>mCherry RNAi
repo>Fer1HCH RNAi
repo>Fer2LCH RNAi
Relative mRNA level
F
22 kDa
Tubulin
55 kDa
G
Relative Fer1HCH level
H
25 kDa
I
Relative Fer2lch level
J
GFP; mCherry RNAi
GFP; Fer1HCH RNAi
Fer1HCH; Fer1HCH RNAi
GFP; Fer2LCH RNAi
Fer2LCH; Fer2LCH RNAi
K
L

Figure 1—figure supplement 1

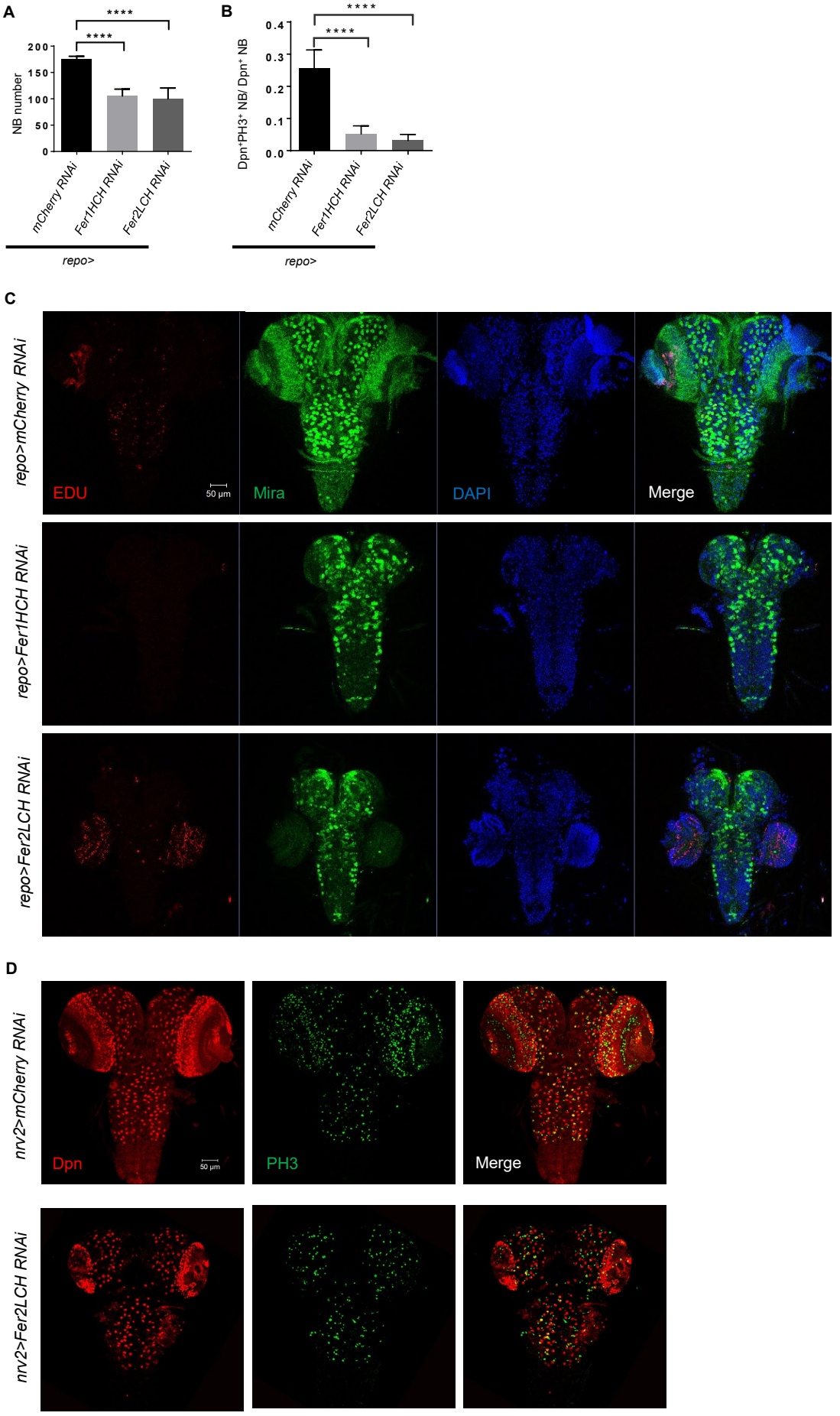

Figure 1—figure supplement 2

A

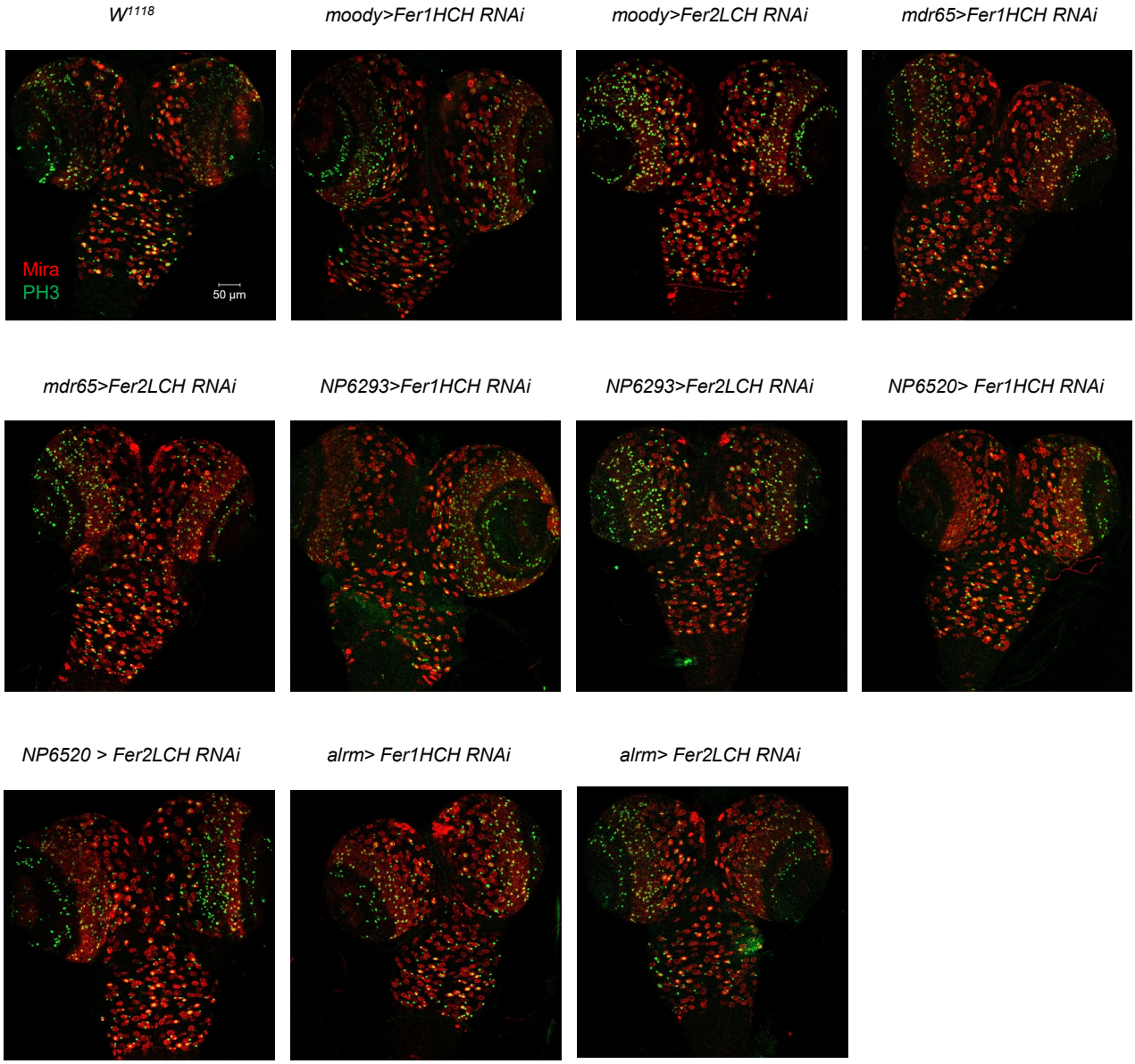

Figure 1—figure supplement 3

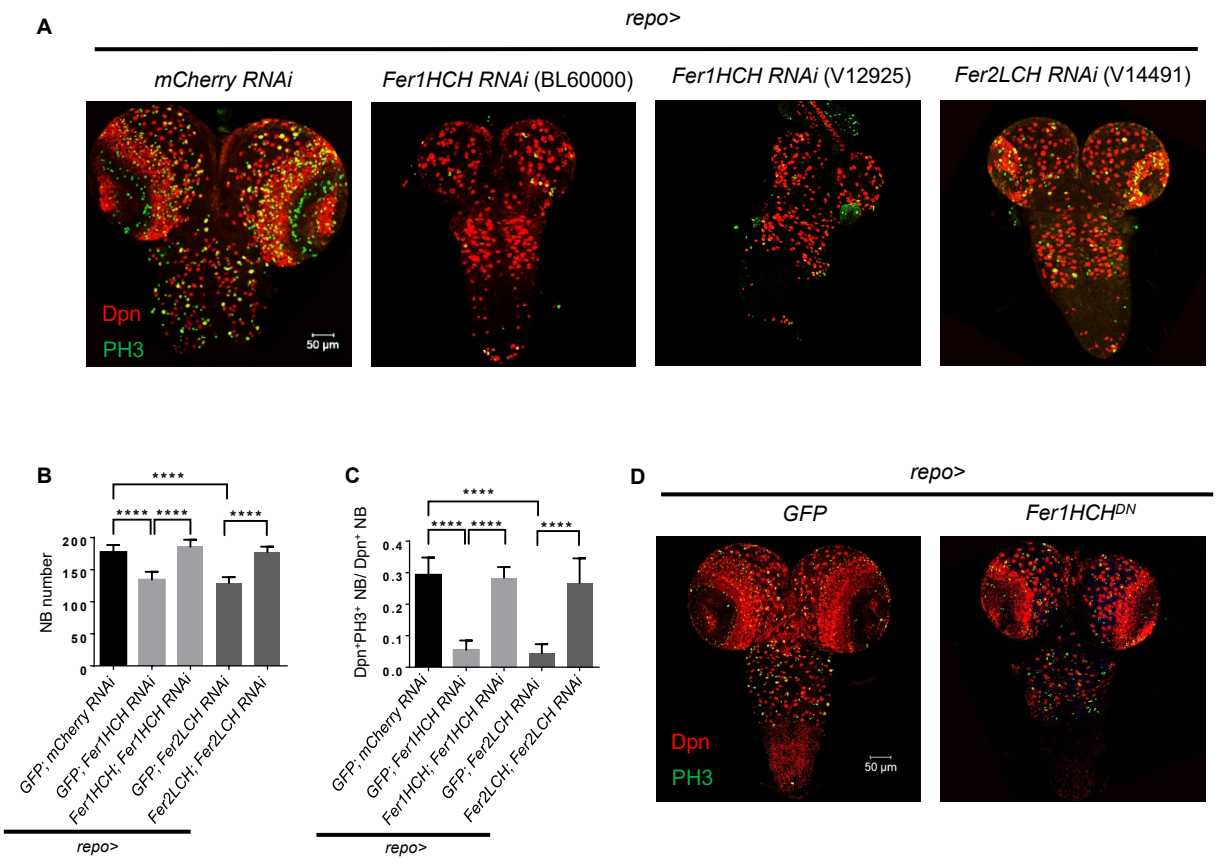

Figure 2

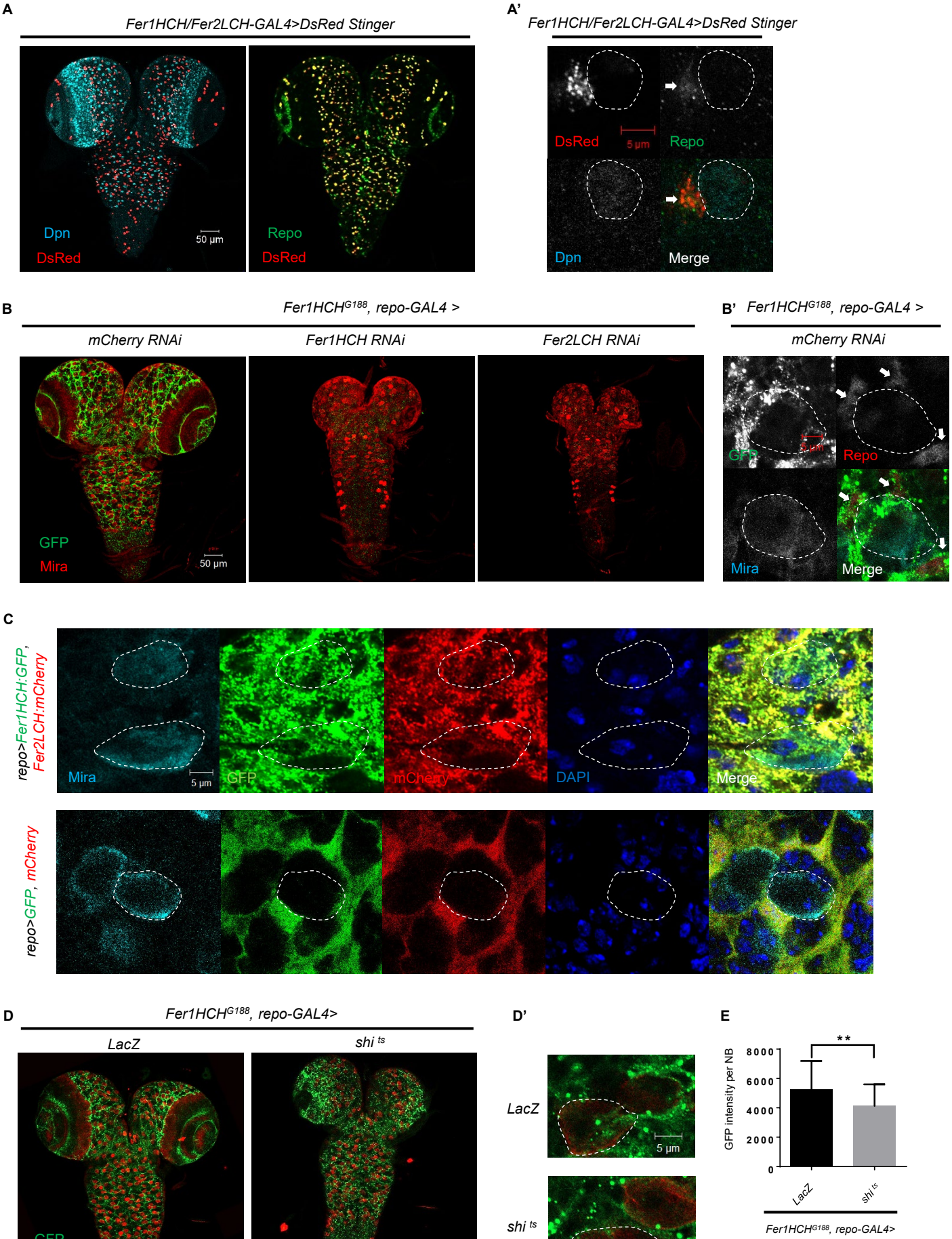
A
Fer1HCH/Fer2LCH-GAL4>DsRed Stinger
Dpn
DsRed
50 µm
Repo
DsRed
A'
Fer1HCH/Fer2LCH-GAL4>DsRed Stinger
DsRed
5 µm
Repo
Dpn
Merge
B
Fer1HCH^G188, repo-GAL4 >
mCherry RNAi
Fer1HCH RNAi
Fer2LCH RNAi
GFP
Mira
50 µm
B'
Fer1HCH^G188, repo-GAL4 >
mCherry RNAi
GFP
5 µm
Repo
Mira
Merge
C
repo>Fer1HCH:GFP, Fer2LCH:mCherry
Mira
5 µm
GFP
mCherry
DAPI
Merge
repo>GFP, mCherry
D
Fer1HCH^G188, repo-GAL4>
LacZ
shi ts
GFP
Dpn
50 µm
D'
LacZ
5 µm
shi ts
E
GFP intensity per NB
8000
6000
4000
2000
0
**
LacZ
shi ts
Fer1HCH^G188, repo-GAL4>

Figure 2—figure supplement 1

A

Fer2LCH-GAL4>DsRed Stinger (DGRC104255)

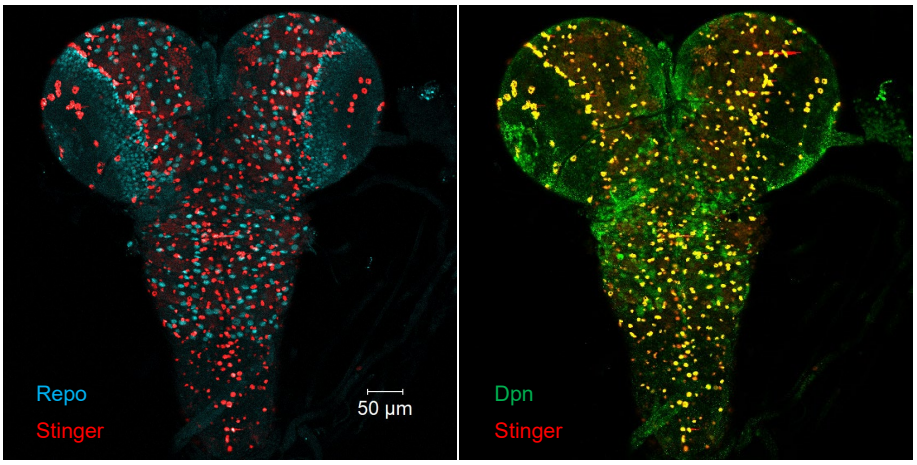

Figure 3

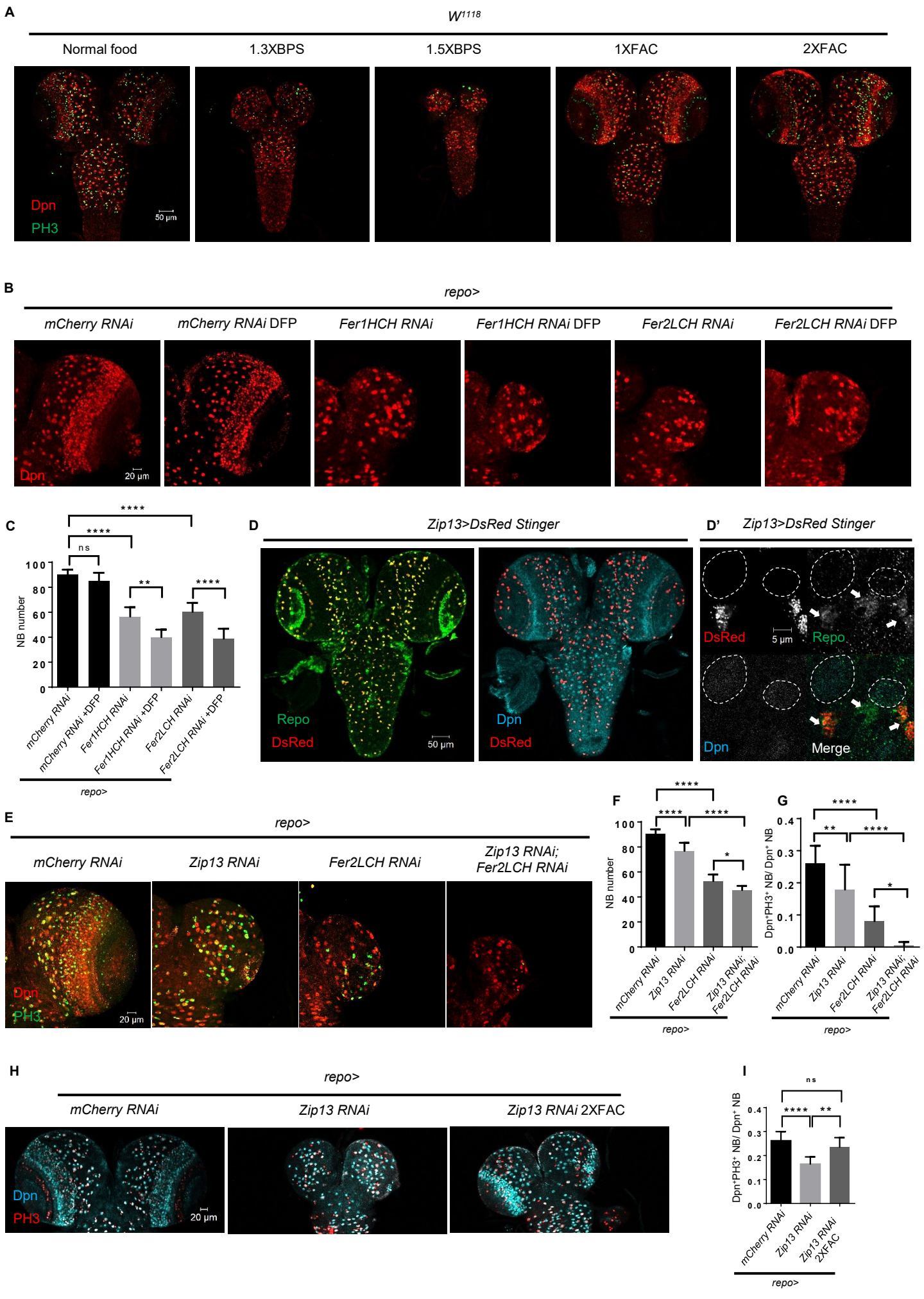
A
W1118
Normal food
1.3XBPS
1.5XBPS
1XFAC
2XFAC
Dpn
PH3
50 µm
B
repo>
mCherry RNAi
mCherry RNAi DFP
Fer1HCH RNAi
Fer1HCH RNAi DFP
Fer2LCH RNAi
Fer2LCH RNAi DFP
Dpn
20 µm
C
NB number
ns
****
**
mCherry RNAi
mCherry RNAi +DFP
Fer1HCH RNAi
Fer1HCH RNAi +DFP
Fer2LCH RNAi
Fer2LCH RNAi +DFP
repo>
D
Zip13>DsRed Stinger
Repo
DsRed
Dpn
50 µm
D'
Zip13>DsRed Stinger
DsRed
5 µm
Repo
Dpn
Merge
E
repo>
mCherry RNAi
Zip13 RNAi
Fer2LCH RNAi
Zip13 RNAi; Fer2LCH RNAi
Dpn
PH3
20 µm
F
NB number
*
G
Dpn+PH3+ NB/ Dpn+ NB
H
repo>
mCherry RNAi
Zip13 RNAi
Zip13 RNAi 2XFAC
Dpn
PH3
20 µm
I
Dpn+PH3+ NB/ Dpn+ NB
Zip13 RNAi 2XFAC

Figure 3—figure supplement 1

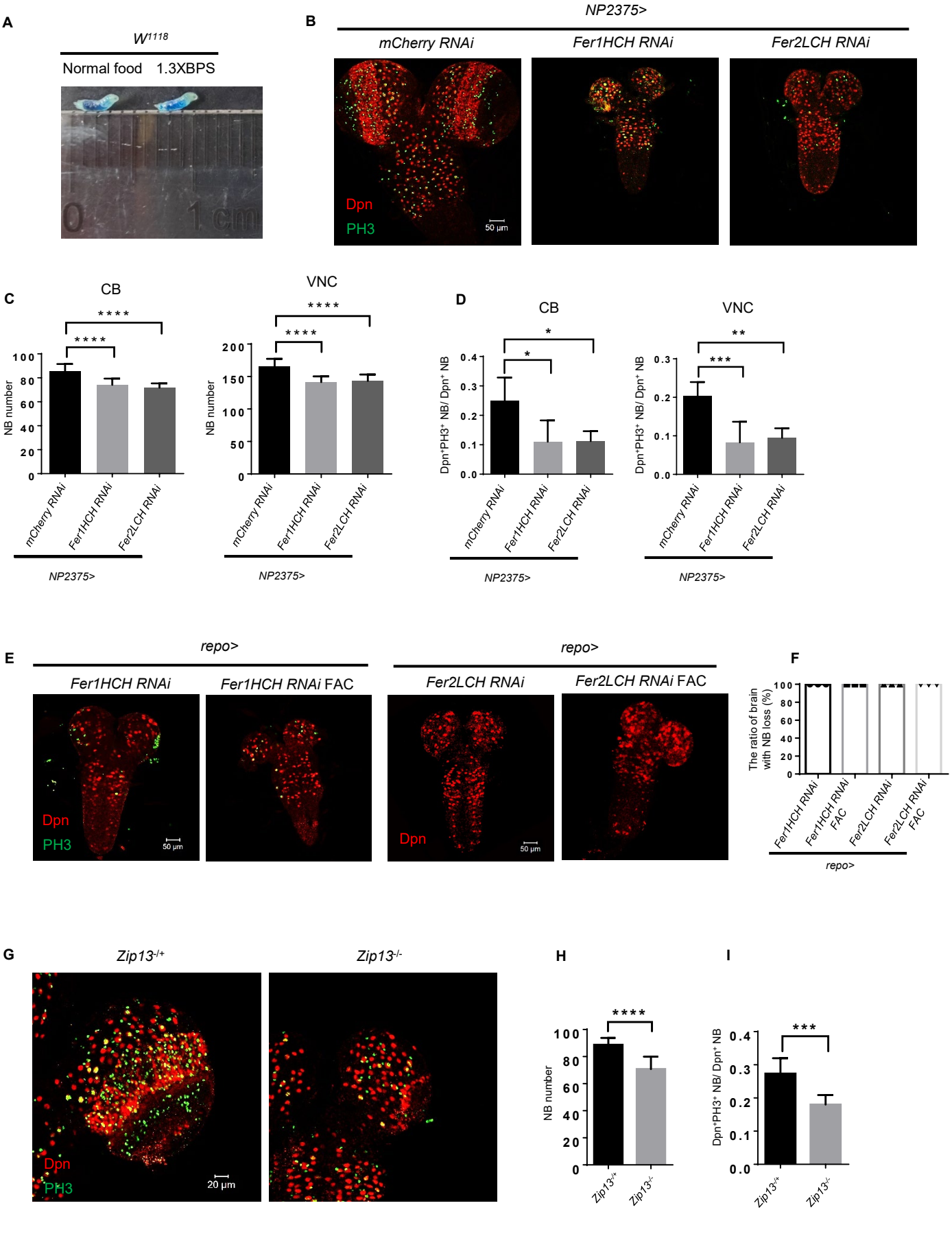

Figure 3—figure supplement 2

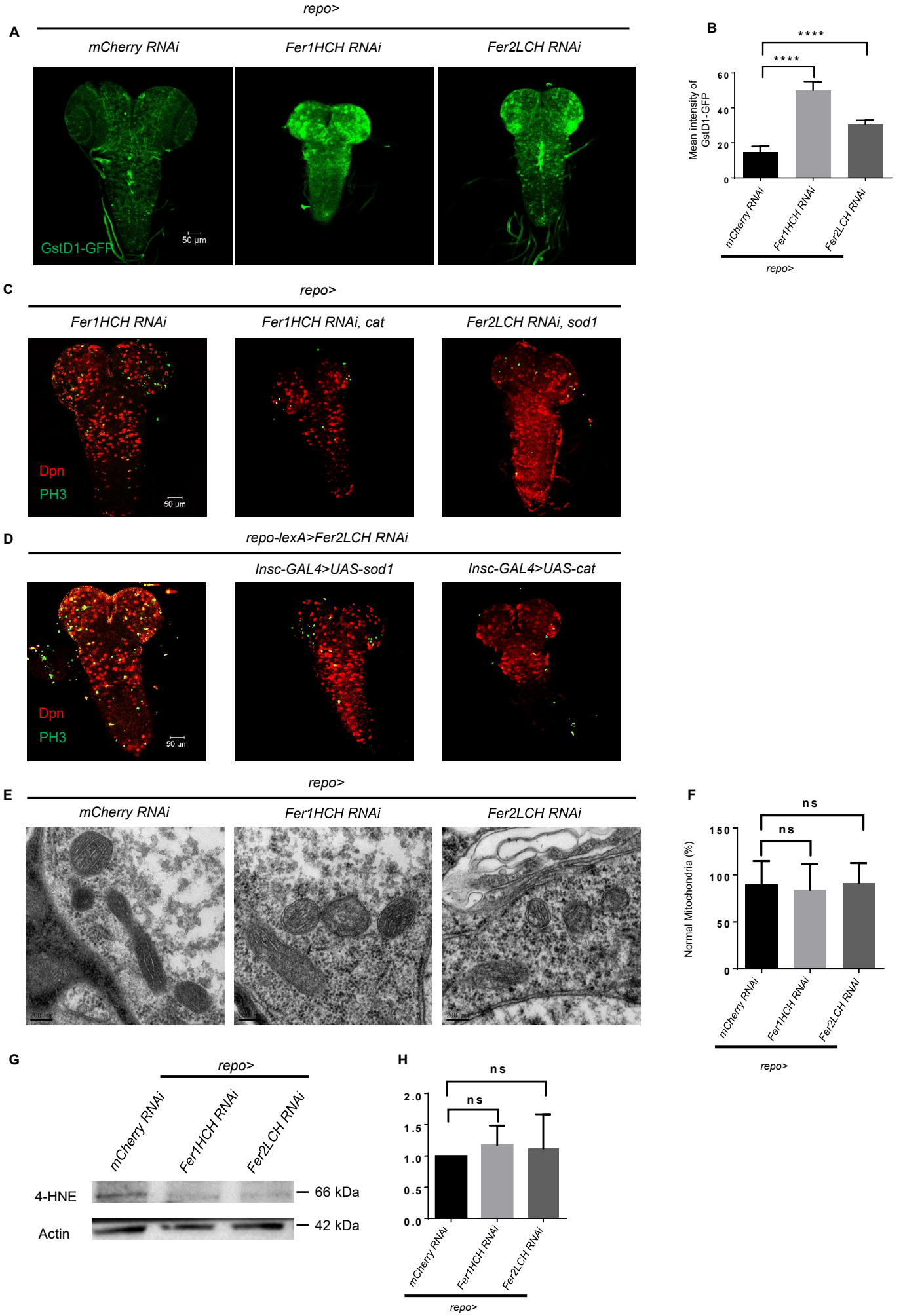

Figure 3—figure supplement 3

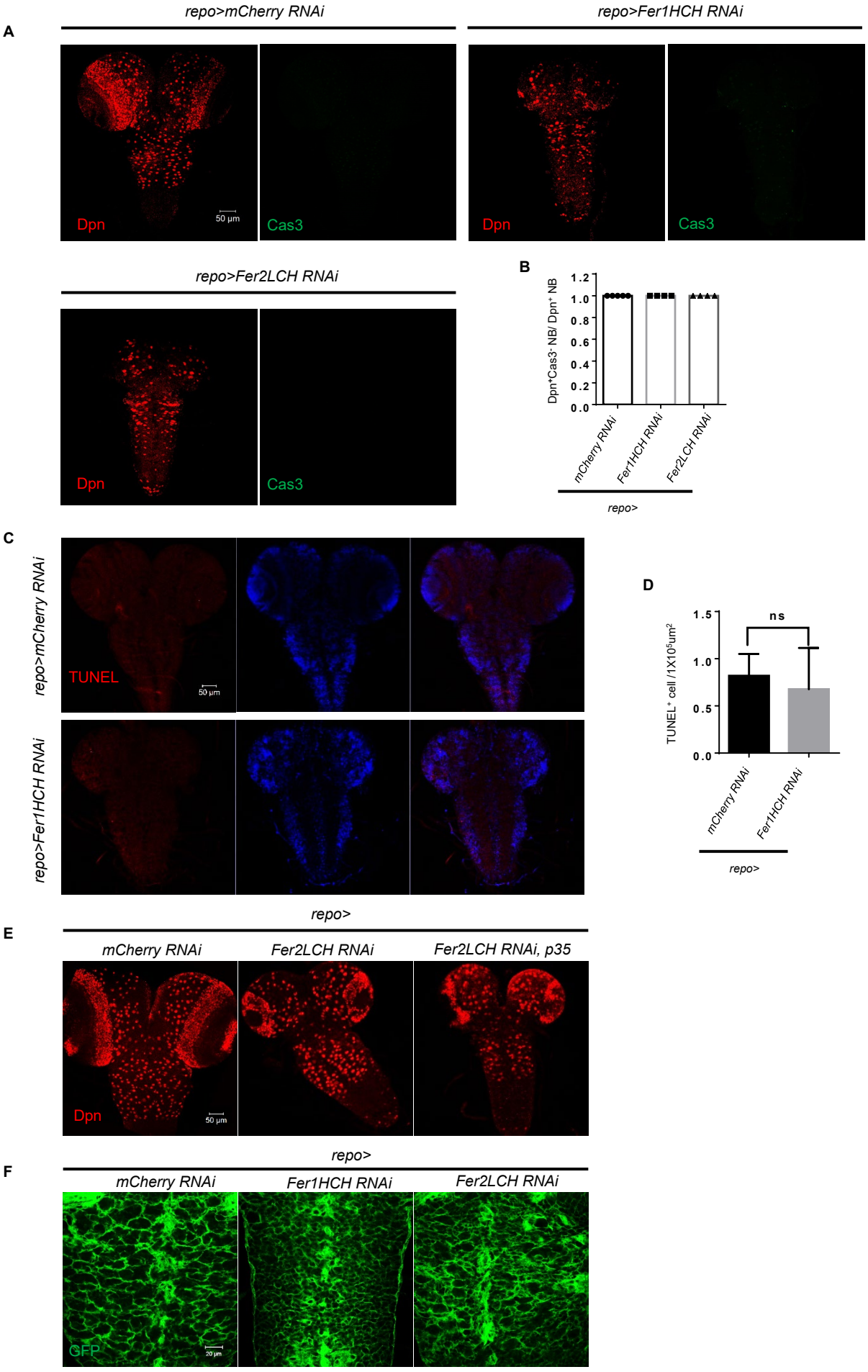

Figure 4

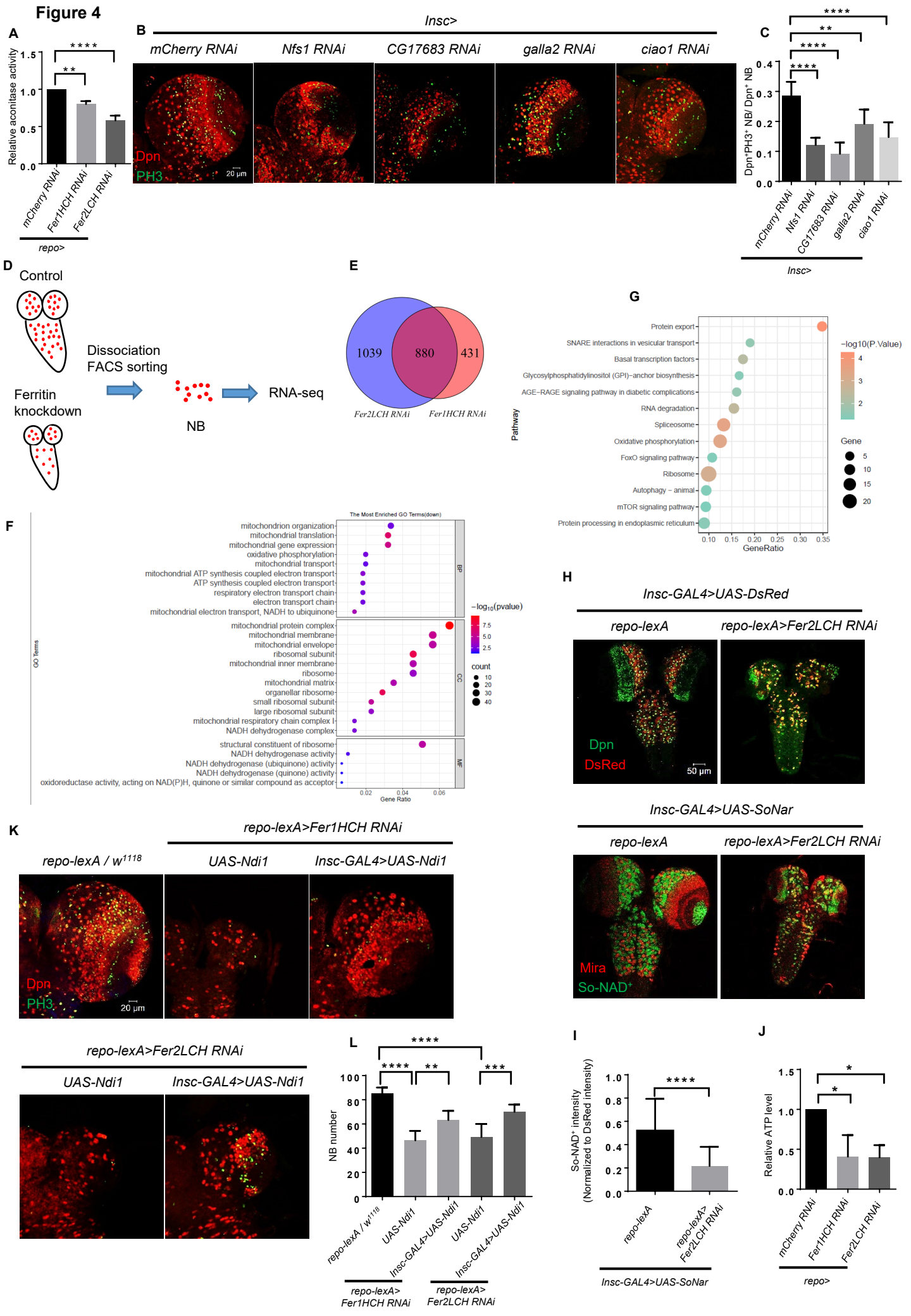
A
Relative aconitase activity
mCherry RNAi
Fer1HCH RNAi
Fer2LCH RNAi
repo>
B
Insc>
mCherry RNAi
Nfs1 RNAi
CG17683 RNAi
galla2 RNAi
ciao1 RNAi
Dpn
PH3
20 μm
C
Dpn+PH3+ NB/ Dpn+ NB
mCherry RNAi
Nfs1 RNAi
CG17683 RNAi
galla2 RNAi
ciao1 RNAi
Insc>
D
Control
Ferritin knockdown
Dissociation
FACS sorting
NB
RNA-seq
E
1039
880
431
Fer2LCH RNAi
Fer1HCH RNAi
G
Protein export
SNARE interactions in vesicular transport
Basal transcription factors
Glycosylphosphatidylinositol (GPI)−anchor biosynthesis
AGE−RAGE signaling pathway in diabetic complications
RNA degradation
Spliceosome
Oxidative phosphorylation
FoxO signaling pathway
Ribosome
Autophagy − animal
mTOR signaling pathway
Protein processing in endoplasmic reticulum
Pathway
GeneRatio
−log10(P.Value)
Gene
F
The Most Enriched GO Terms(down)
mitochondrion organization
mitochondrial translation
mitochondrial gene expression
oxidative phosphorylation
mitochondrial transport
mitochondrial ATP synthesis coupled electron transport
ATP synthesis coupled electron transport
respiratory electron transport chain
electron transport chain
mitochondrial electron transport, NADH to ubiquinone
mitochondrial protein complex
mitochondrial membrane
mitochondrial envelope
ribosomal subunit
mitochondrial inner membrane
ribosome
mitochondrial matrix
organellar ribosome
small ribosomal subunit
large ribosomal subunit
mitochondrial respiratory chain complex I
NADH dehydrogenase complex
structural constituent of ribosome
NADH dehydrogenase activity
NADH dehydrogenase (ubiquinone) activity
NADH dehydrogenase (quinone) activity
oxidoreductase activity, acting on NAD(P)H, quinone or similar compound as acceptor
BP
CC
MF
GO Terms
Gene Ratio
−log10(pvalue)
count
H
Insc-GAL4>UAS-DsRed
repo-lexA
repo-lexA>Fer2LCH RNAi
Dpn
DsRed
50 μm
Insc-GAL4>UAS-SoNar
repo-lexA
repo-lexA>Fer2LCH RNAi
Mira
So-NAD+
K
repo-lexA>Fer1HCH RNAi
repo-lexA / w1118
UAS-Ndi1
Insc-GAL4>UAS-Ndi1
Dpn
PH3
20 μm
repo-lexA>Fer2LCH RNAi
UAS-Ndi1
Insc-GAL4>UAS-Ndi1
L
NB number
repo-lexA / w1118
UAS-Ndi1
Insc-GAL4>UAS-Ndi1
UAS-Ndi1
Insc-GAL4>UAS-Ndi1
repo-lexA> Fer1HCH RNAi
repo-lexA> Fer2LCH RNAi
I
So-NAD+ intensity (Normalized to DsRed intensity)
repo-lexA
repo-lexA> Fer2LCH RNAi
Insc-GAL4>UAS-SoNar
J
Relative ATP level
mCherry RNAi
Fer1HCH RNAi
Fer2LCH RNAi
repo>

Figure 4—figure supplement 1

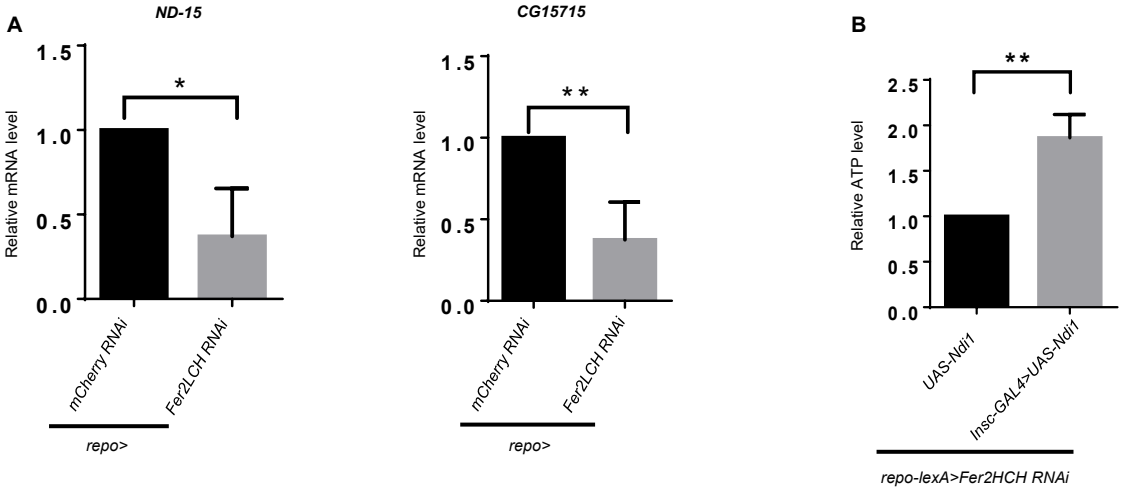

Figure 5

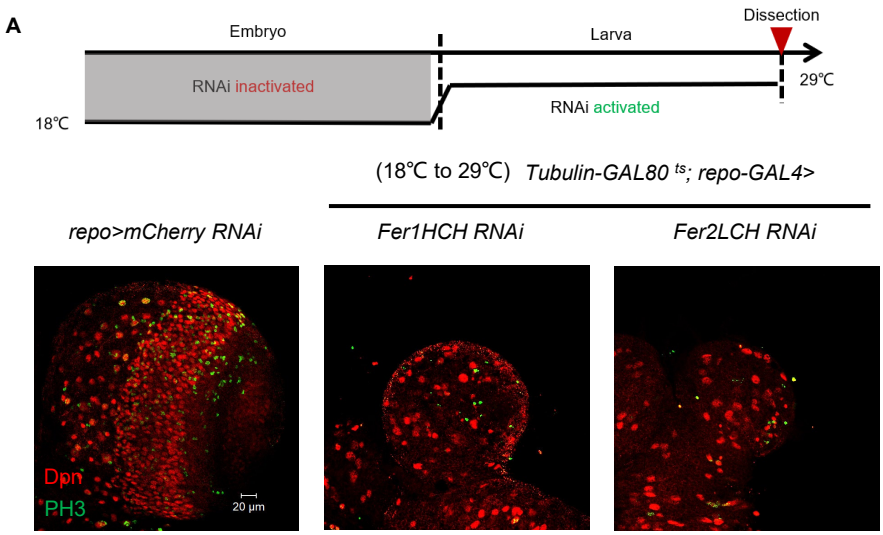
A
Embryo
Larva
Dissection
RNAi inactivated
RNAi activated
18℃
29℃
(18℃ to 29℃) Tubulin-GAL80 ts; repo-GAL4>
repo>mCherry RNAi
Fer1HCH RNAi
Fer2LCH RNAi
Dpn
PH3
20 μm

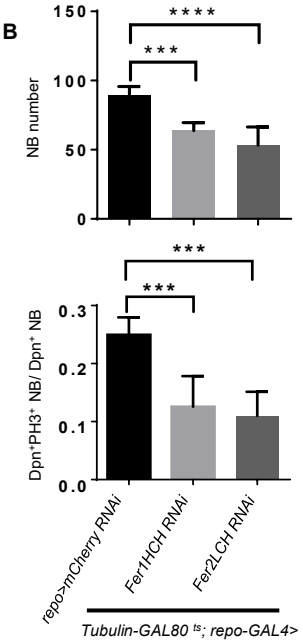
B
NB number
150
100
50
0
****
***
Dpn+PH3+ NB/ Dpn+ NB
0.3
0.2
0.1
0.0
***
***
repo>mCherry RNAi
Fer1HCH RNAi
Fer2LCH RNAi
Tubulin-GAL80 ts; repo-GAL4>

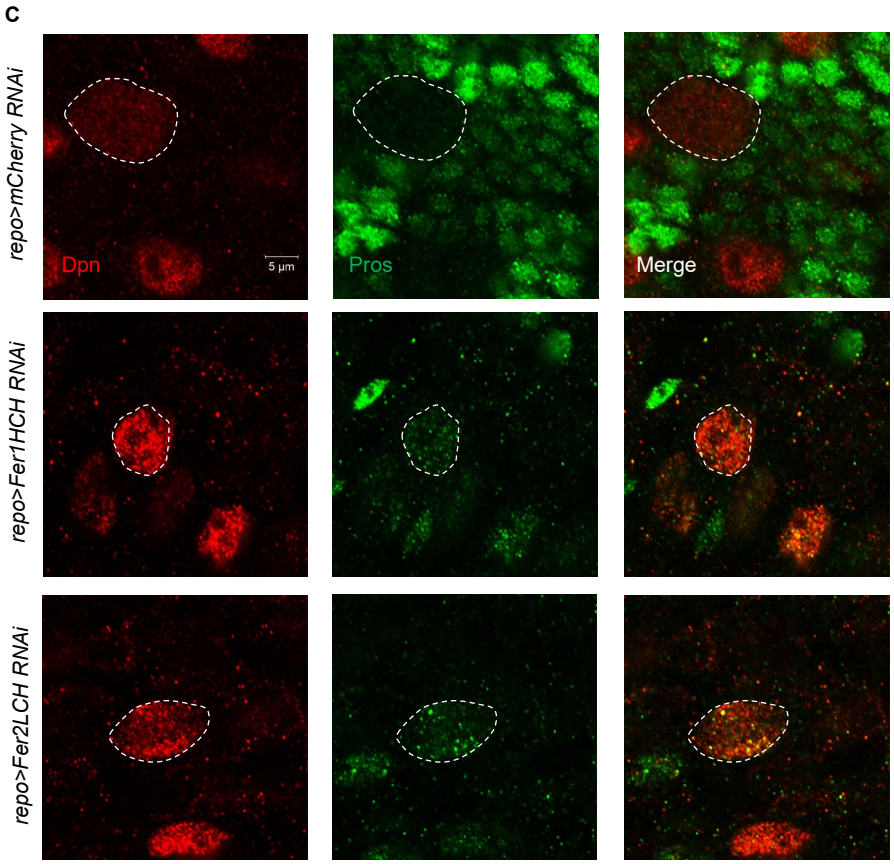
C
repo>mCherry RNAi
repo>Fer1HCH RNAi
repo>Fer2LCH RNAi
Dpn
5 μm
Pros
Merge

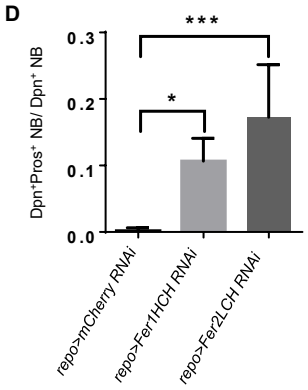
D
Dpn+Pros+ NB/ Dpn+ NB
0.3
0.2
0.1
0.0
***
*
repo>mCherry RNAi
repo>Fer1HCH RNAi
repo>Fer2LCH RNAi

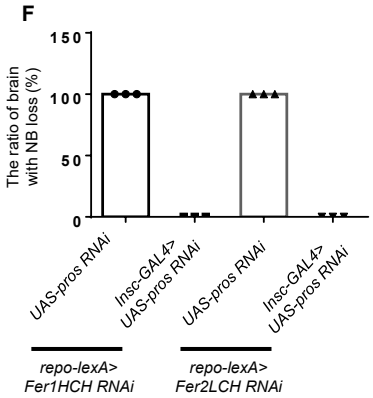
F
The ratio of brain with NB loss (%)
150
100
50
0
UAS-pros RNAi
Insc-GAL4> UAS-pros RNAi
UAS-pros RNAi
Insc-GAL4> UAS-pros RNAi
repo-lexA> Fer1HCH RNAi
repo-lexA> Fer2LCH RNAi

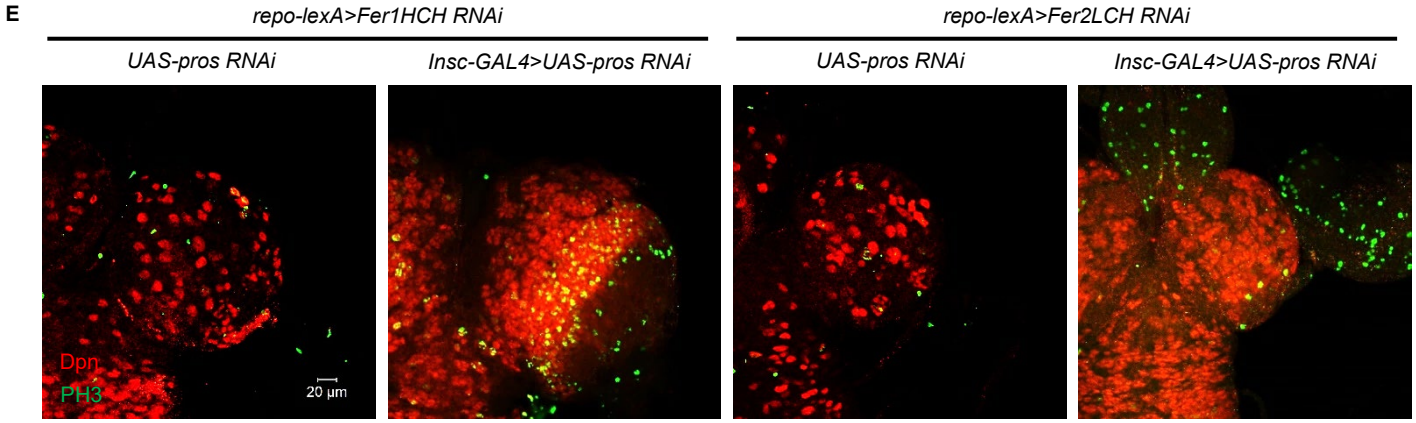
E
repo-lexA>Fer1HCH RNAi
repo-lexA>Fer2LCH RNAi
UAS-pros RNAi
Insc-GAL4>UAS-pros RNAi
UAS-pros RNAi
Insc-GAL4>UAS-pros RNAi
Dpn
PH3
20 μm

Figure 5—figure supplement 1

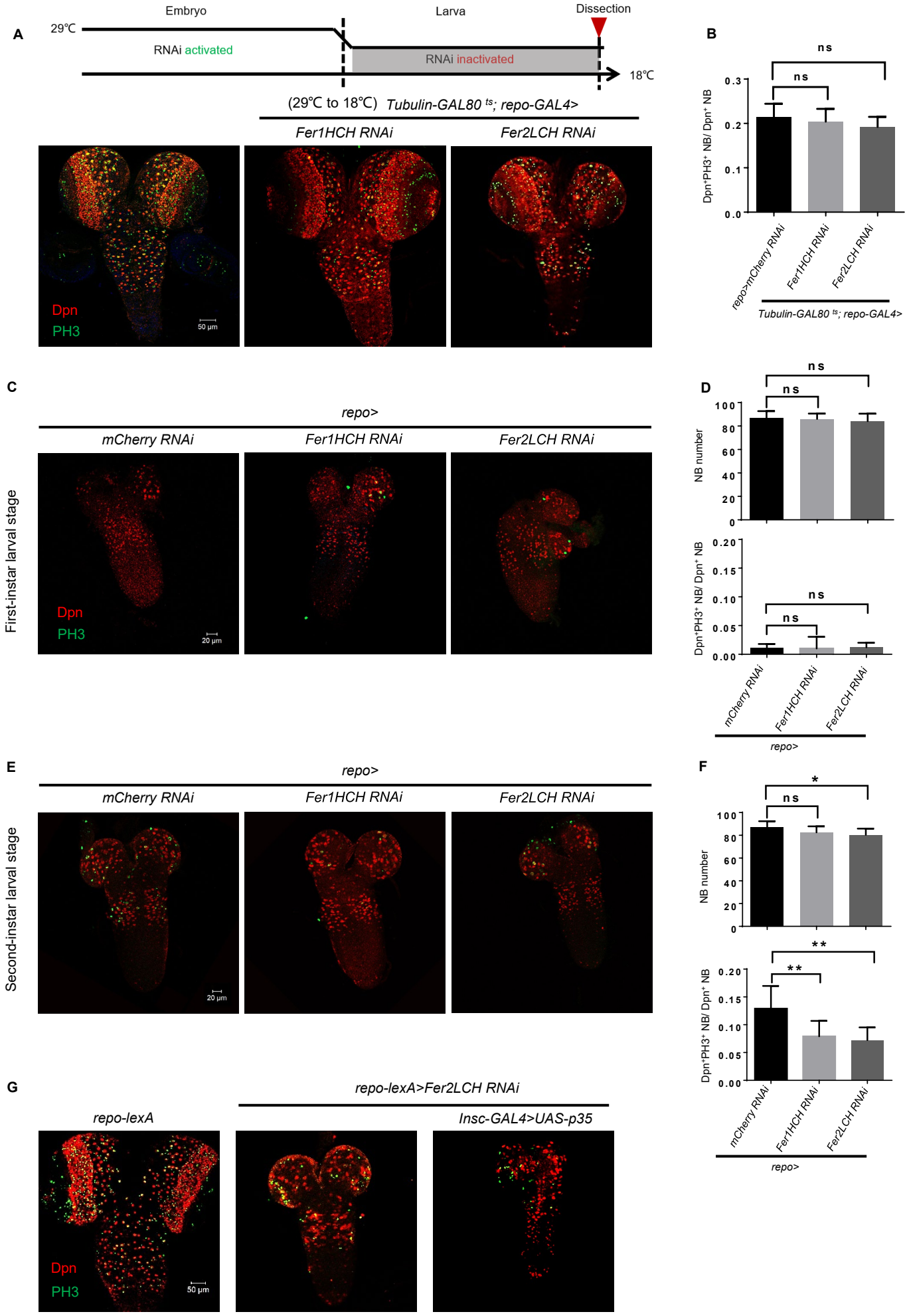

Figure 5—figure supplement 2

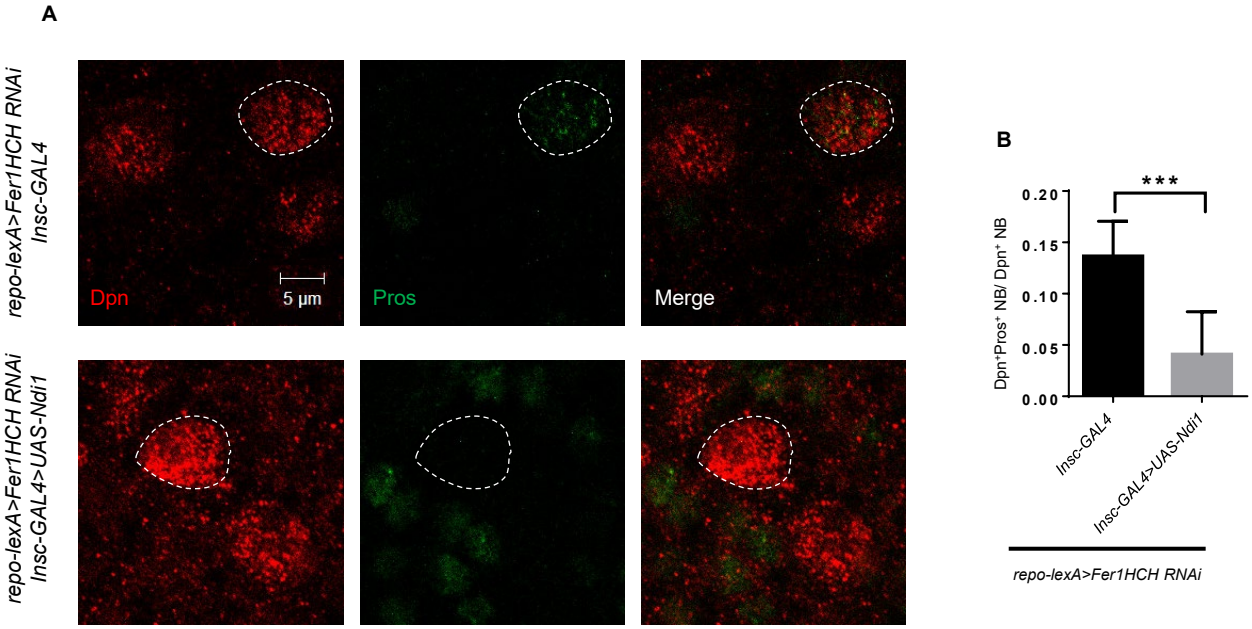

Figure 5—figure supplement 3

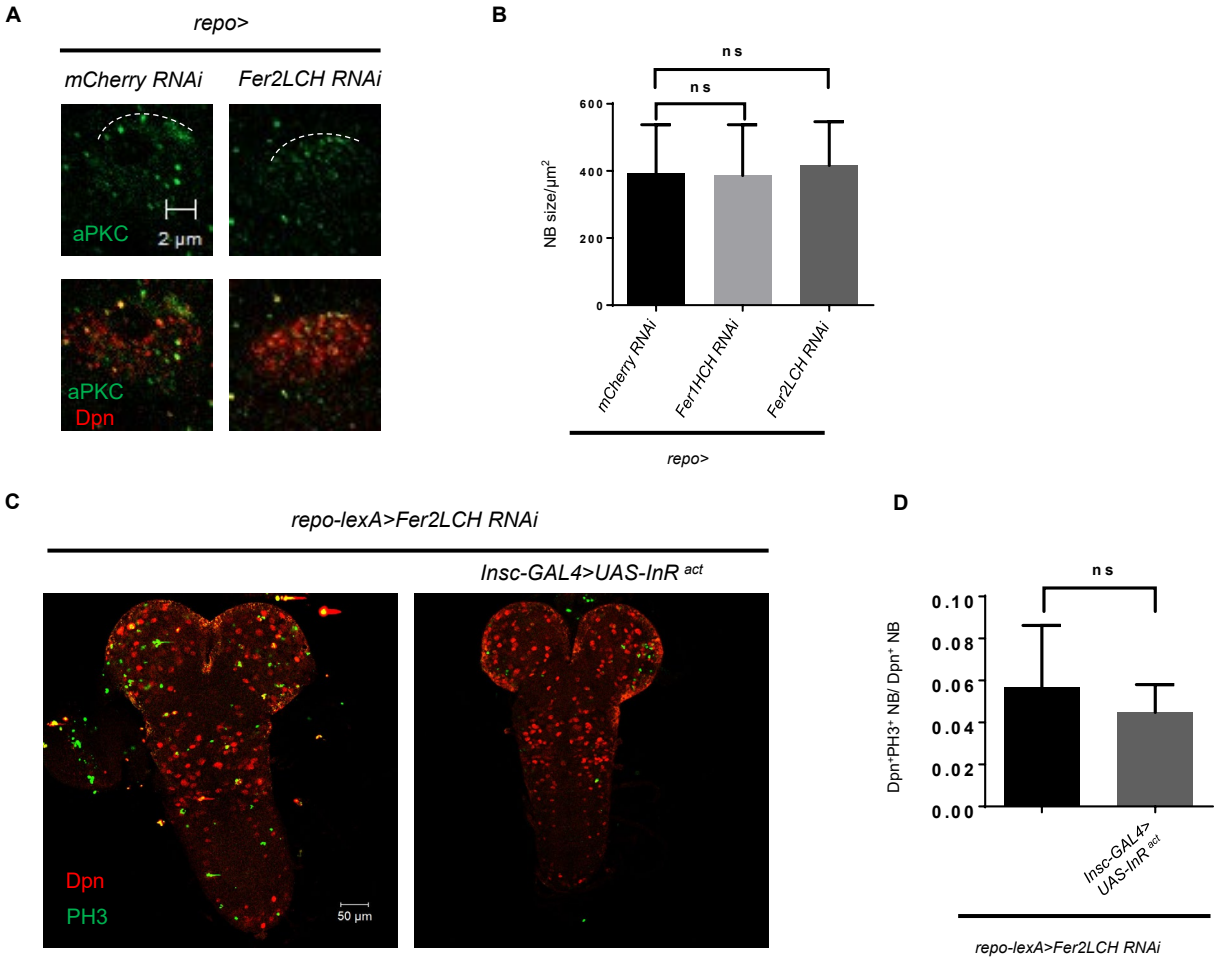

Figure 6

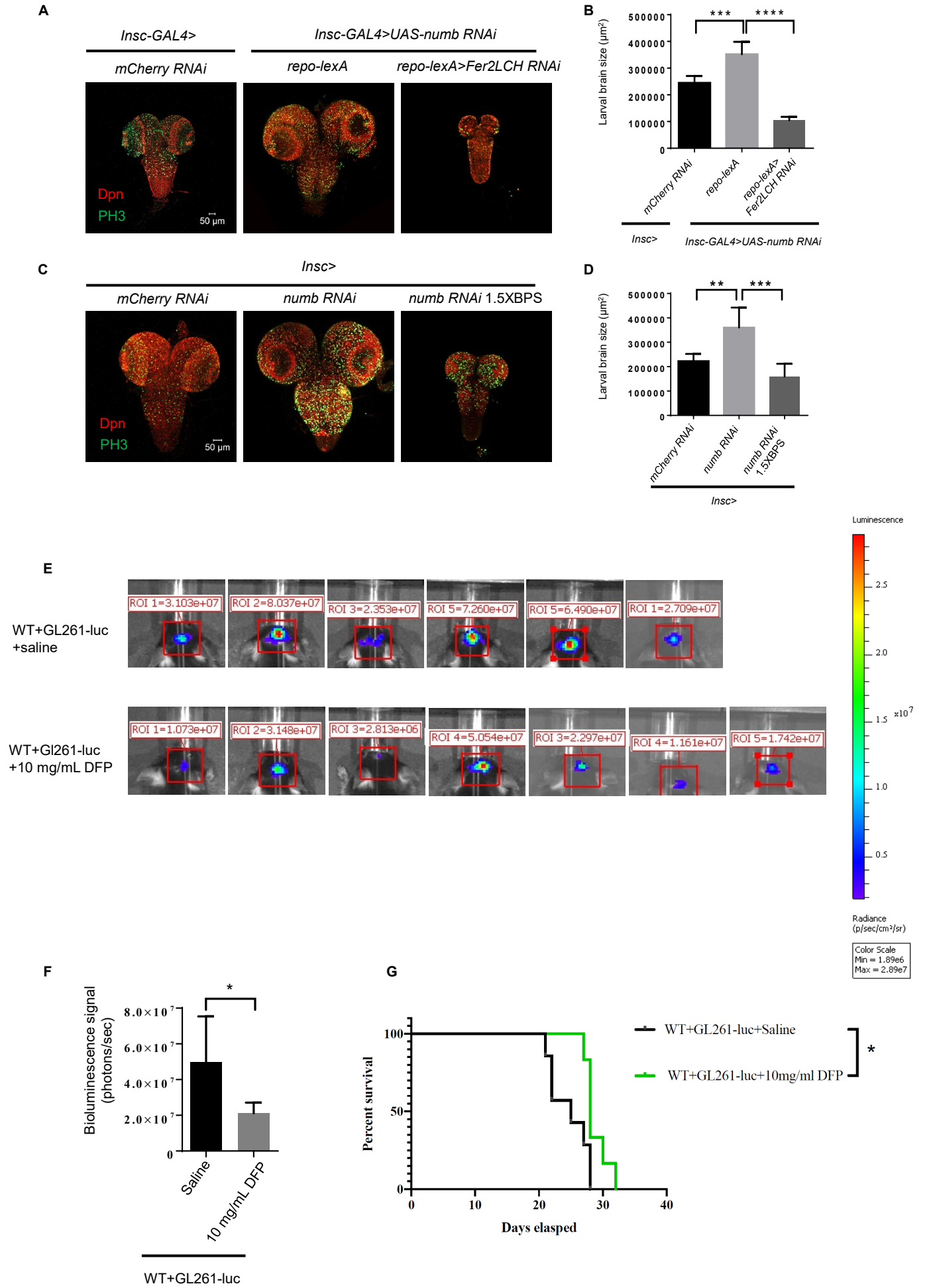
A
Insc-GAL4>
Insc-GAL4>UAS-numb RNAi
mCherry RNAi
repo-lexA
repo-lexA>Fer2LCH RNAi
Dpn
PH3
50 µm
B
Larval brain size (µm²)
500000
400000
300000
200000
100000
0
***
****
mCherry RNAi
repo-lexA
repo-lexA> Fer2LCH RNAi
Insc>
Insc-GAL4>UAS-numb RNAi
C
Insc>
mCherry RNAi
numb RNAi
numb RNAi 1.5XBPS
Dpn
PH3
50 µm
D
Larval brain size (µm²)
500000
400000
300000
200000
100000
0
**
***
mCherry RNAi
numb RNAi
numb RNAi 1.5XBPS
Insc>
E
WT+GL261-luc +saline
ROI 1=3.103e+07
ROI 2=8.037e+07
ROI 3=2.353e+07
ROI 5=7.260e+07
ROI 5=6.490e+07
ROI 1=2.709e+07
WT+Gl261-luc +10 mg/mL DFP
ROI 1=1.073e+07
ROI 2=3.148e+07
ROI 3=2.813e+06
ROI 4=5.054e+07
ROI 3=2.297e+07
ROI 4=1.161e+07
ROI 5=1.742e+07
Luminescence
2.5
2.0
1.5
1.0
0.5
x10⁷
Radiance (p/sec/cm²/sr)
Color Scale
Min = 1.89e6
Max = 2.89e7
F
Bioluminescence signal (photons/sec)
8.0×10⁷
6.0×10⁷
4.0×10⁷
2.0×10⁷
0
*
Saline
10 mg/mL DFP
WT+GL261-luc
G
Percent survival
100
50
0
0
10
20
30
40
Days elasped
WT+GL261-luc+Saline
WT+GL261-luc+10mg/ml DFP
*

Figure 6—figure supplement 1

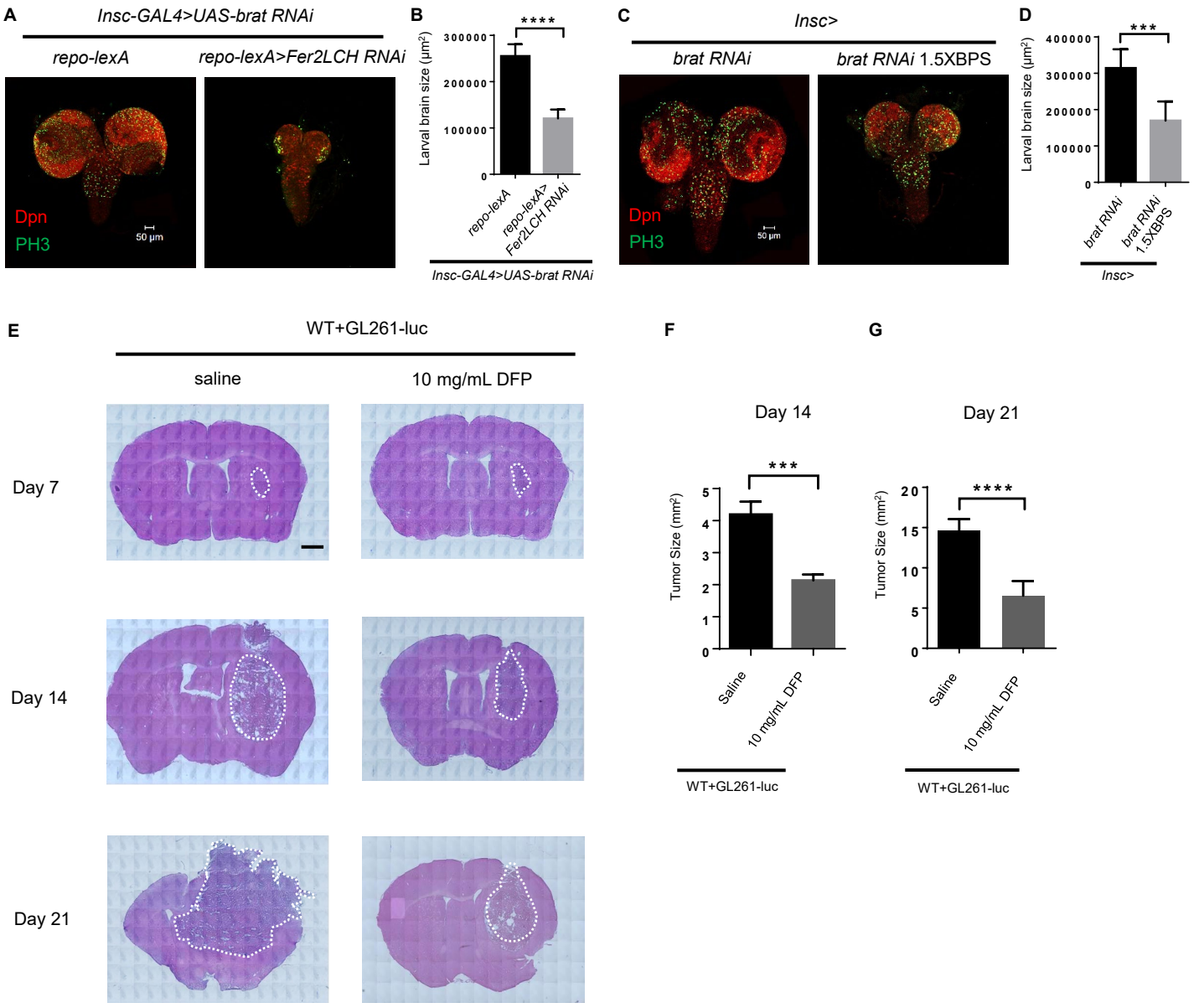

Figure 7

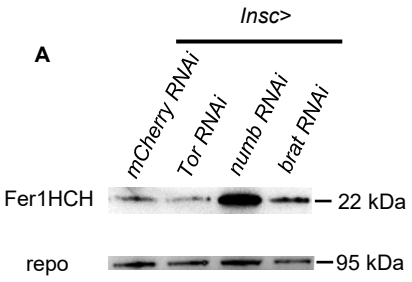
A
Insc>
mCherry RNAi
Tor RNAi
numb RNAi
brat RNAi
Fer1HCH
22 kDa
repo
95 kDa

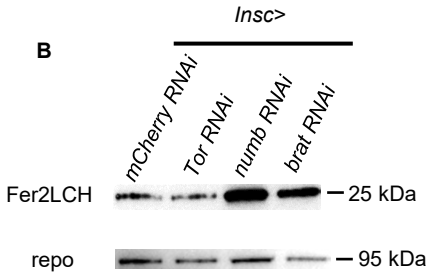
B
Insc>
mCherry RNAi
Tor RNAi
numb RNAi
brat RNAi
Fer2LCH
25 kDa
repo
95 kDa

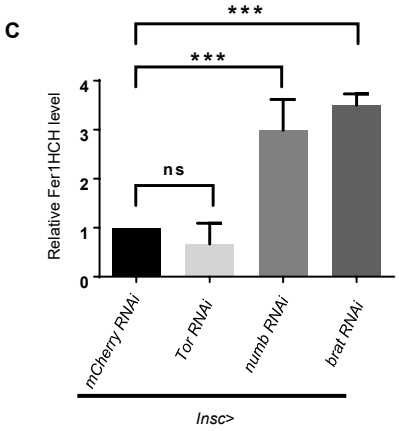
C
***
***
ns
Relative Fer1HCH level
0
1
2
3
4
mCherry RNAi
Tor RNAi
numb RNAi
brat RNAi
Insc>

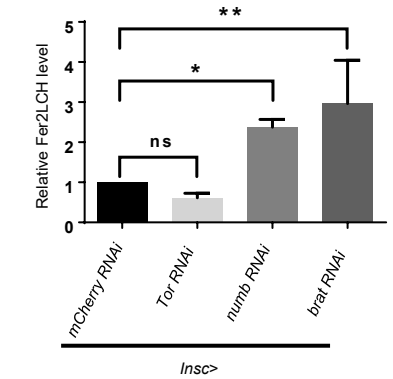
D
**
*
ns
Relative Fer2LCH level
0
1
2
3
4
5
mCherry RNAi
Tor RNAi
numb RNAi
brat RNAi
Insc>

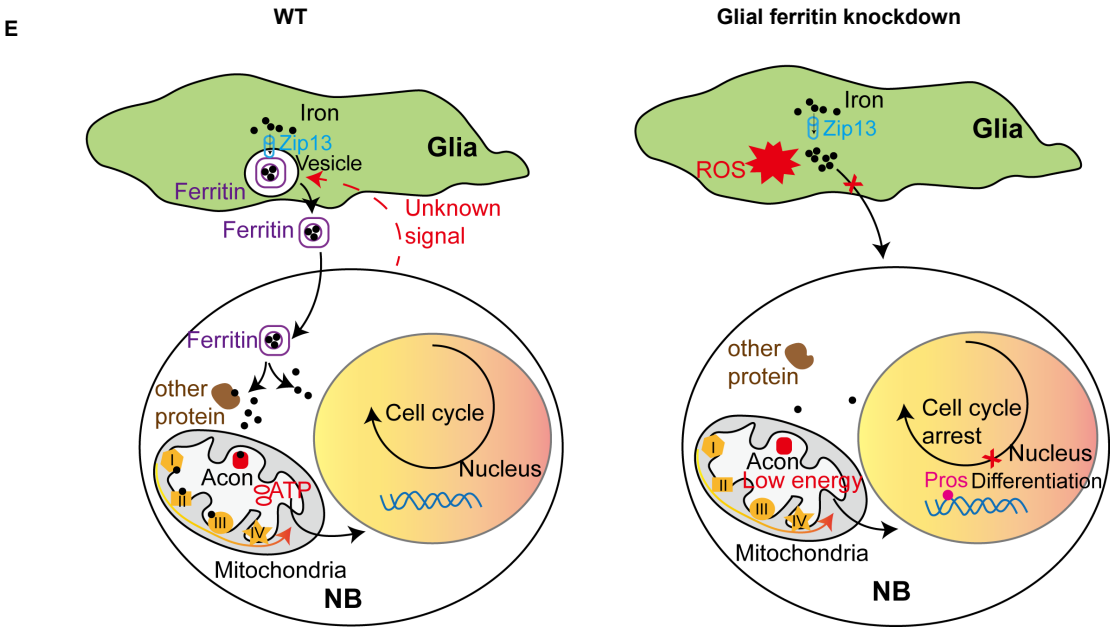
E
WT
Glial ferritin knockdown
Iron
Zip13
Glia
Vesicle
Ferritin
Unknown signal
Ferritin
Ferritin
other protein
Cell cycle
Nucleus
Acon
ATP
I
II
III
IV
Mitochondria
NB
Iron
Zip13
Glia
ROS
other protein
Cell cycle arrest
Nucleus
Acon
Low energy
Pros
Differentiation
I
II
III
IV
Mitochondria
NB